Binuclear Dithiocarbamate Macrocyclic Complexes of Ni^{II}, Zn^{II} and Cd^{II} Derived From 4,4'-Bis(arylmethylamino) diphenyl ether, CS_2 and $M(OAc)_2$: Synthesis, Characterization, DFT study and *in vitro* Cytotoxicity

Abstract

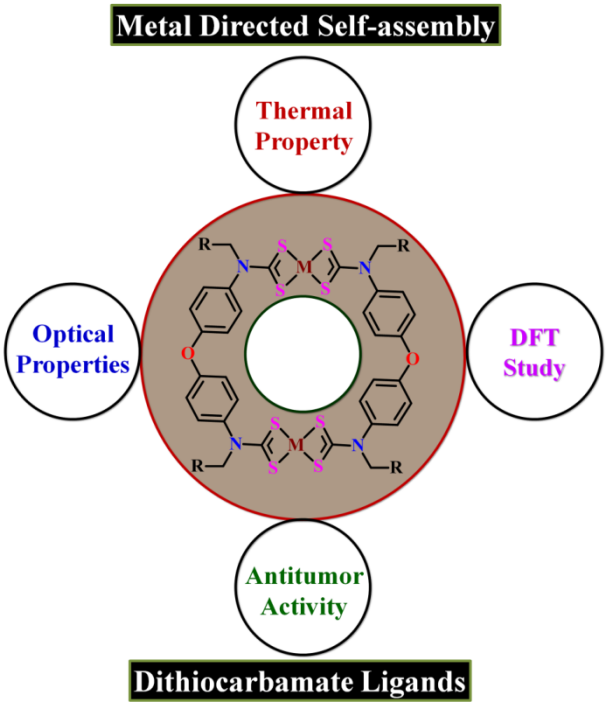

A series of bimetallic dithiocarbamate macrocyclic complexes [M^{II}_2-μ^2-bis-{(κ^2S,S-$S_2CN(R)C_6H_4)_2O$}].L {R = -benzyl; M =Ni^{II} **1**, Zn^{II} **2**, Cd^{II} **3**; R = 1-naphthylmethyl; M =Ni^{II} **4**, Zn^{II} **5**, Cd^{II} **6** and L = Et_3N for **1**, **4** only} were efficiently synthesized through self-assembly process involving the 4,4'-bis(arylmethylamino)diphenyl ethers $\mathbf{L^1}$-$\mathbf{L^2}$, CS_2 and $M(OAc)_2$. These were characterized by micro-, relevant spectroscopic and TGA/DTA analyses. Geometry of all the complexes has been optimized by DFT method. Complexes **1-6** were studied for their optical properties and *in vitro* cytotoxicity against HEP 3B and IMR 32 by the MTT assay. These macrocyclic scaffolds were found active against both the cell lines and cytotoxicity data confirms better potency than cisplatin, in which binuclear Ni^{II}dithiocarbamate macrocycle **1** exhibits optimum cytotoxicity. Job plot experiment reveals the ability of macrocycle **4** to form intramolecular 1:1 host–guest inclusion complex with bidentate guests 1,4-dioxane and piperazine.

5B.1. Introduction

A wide range of dithiocarbamate complexes prepared exhibit several interesting physicochemical propertiesand diverse applicability,[1,2] especially in the field of supramolecular chemistry.[1] Beer and co-workers have contributed much in preparing a range of exciting new supramolecular architectures including macrocyclic based on multifunctional dithiocarbamate ligands, many of them show interesting structural, redox properties.[1] Reportedly, dithiocarbamate moiety found of great biological significance showing excellent medicinal activity like antibiotic, anticancer activity.

Despite of the valuable stereoelectronic characteristics and a ground breaking success of dithiocarbamate based macrocyclic complexes in supramolecular chemistry, especially host-guest reactivity study,[2] this structural class (binuclear M^{II}dithiocarbamate macrocyclic complexes) is surprisingly underexploited till today in medicinal chemistry especially for anticancer activity.

Thus, in the light of these observations and potential antitumor activity exhibited by diamine derivatives of 4,4-diaminodiphenyl ether,[3] it was pertinent to use 4,4'-bis(arylmethylamino)diphenyl ethers **L^1-L^2** for further functionalization to achieve better cytotoxicity. The incorporation of biologically active 4,4'-bis(arylmethylamino)diphenyl ether and dithiocarbamate moieties together in the macrocyclic framework is expected to enhance the antitumor activity to great extent. Thus, to explore newer dimensions of metal based macrocyclic architectures, a series of binuclear M^{II}dithiocarbamate macrocyclic complexes **1-6** bearing –($H_4C_6OC_6H_4$)– linker have been designed and synthesized.

In this contribution we report on the synthesis, spectroscopic characterization, optical properties, DFT calculations and *in vitro* cytotoxicity against human cancer cell lines **HEP 3B** (hepatoma) and **IMR 32** (neuroblastoma) of a series of binuclear M^{II}dithiocarbamate macrocyclic complexes [M^{II}_2-μ^2-bis-{(κ^2*S*,*S*-$S_2CN(R)C_6H_4)_2O$}].L {R = -benzyl; M =Ni^{II} **1**, Zn^{II} **2**, Cd^{II} **3**; R = 1-naphthylmethyl; M =Ni^{II} **4**, Zn^{II} **5**, Cd^{II} **6** and L = Et_3N for **1**, **4** only}. The ease of synthesis and interesting *in vitro* antitumor activity against human cancer cell lines HEP 3B and IMR 32 and their potential to form intramolecular 1:1 inclusion complex with bidentate guests add merit to present series of macrocyclic complexes.

5B.2. Experimental Section

5B.2.1. Synthesis of binuclear M^{II}dithiocarbamate macrocyclic complexes 1-6

To a triethyl amine solution of 1 equivalent of respective diamine precursors (200 mg, 0.526 mmol) of $\mathbf{L^1}$ or (252 mg, 0.526 mmol) of $\mathbf{L^2}$), an excess amount of carbon disulfide (~10 equivalent; ~ 0.5 mL) was added with vigorous stirring. The mixture was stirred further for 12 h at room temperature, during this time period, a change in color from colorless to pale yellow was observed. To this reaction mixture, $Ni^{II}(C_2H_3O_2)_2.4H_2O$ (157 mg, 0.6312 mmol), $Zn^{II}(C_2H_3O_2)_2.2H_2O$ (139 mg, 0.6312 mmol) or $Cd^{II}(C_2H_3O_2)_2.4H_2O$ (168 mg, 0.6312 mmol) dissolved in a minimum amount of distilled water was added with rigorous stirring and the reaction was allowed to continue for 8 h at room temperature. The reaction mixture was dried under vacuum and the sticky residue was washed several times with rigorous stirring by distilled water, followed by n-hexane and diethyl ether. At the end, a free flowing powder obtained was dried under vacuum for several hours to yield the corresponding products **1-6** quantitatively, stored under a nitrogen atmosphere and samples were taken for analysis. The synthetic methodology is outlined in Scheme 1.

Table 1. Micro-, mass- and IR analysis data for compounds $\mathbf{L^1}$-$\mathbf{L^6}$ and **1-6**.

Entry	Molecular Formula (MW)	Yield (%)	Mp (°C)	Elemental Analysis (%) Found (calculated)				ES-MS (m/z)	IR data (KBr disk) υ_{max}/cm^{-1}
				C	H	N	S		
1	$C_{62}H_{59}N_5Ni_2O_2S_8$ (1280.07)	85	>110 dec.	58.35 (58.17)	4.72 (4.65)	5.50 (5.47)	19.97 (20.04)	1279.7 $[M.Et_3N+H]^+$	2990w, 2975w, 2960w, 2360m, 1592m, 1495s, 1448s, 1352m, 1240s, 1199s, 1161m, 1076m, 1028w, 1009w, 962s, 873w, 833s, 722m, 697s, 630m, 552m.
2	$C_{56}H_{44}N_4O_2S_8Zn_2$ (1192.25)	93	>140 dec.	56.45 (56.41)	3.75 (3.72)	4.69 (4.70)	21.50 (21.52)	1213.3 $[M+Na]^+$	3028w, 2977w, 2924w, 2360w, 2350w, 1591m, 1550m, 1496s, 1441m, 1393s, 1351m, 1239s, 1201s, 1161m, 1078m, 1011w, 962m, 873w, 832m, 724m, 698s, 650w, 554w, 514w.
3	$C_{56}H_{44}Cd_2N_4O_2S_8$ (1286.32)	89	>90 dec.	52.35 (52.29)	3.57 (3.45)	4.33 (4.36)	19.90 (19.94)	1320.5 $[M+Cl]^-$	3027w, 2977w, 2666w, 1602w, 1495s, 1450w, 1434w, 1385m, 1448w, 1238s, 1200s, 1160m, 1078m, 963m, 873w, 833m, 725w, 699m, 647w, 553w, 454w.
4	$C_{78}H_{67}N_5Ni_2O_2S_8$ (1480.31)	81	>150 dec.	63.50 (63.29)	4.75 (4.56)	4.70 (4.73)	17.29 (17.33)	1343.3 $[(M-S)+H]^+$	3042w, 2976m, 2939m, 2738w, 2675m, 2603m, 2495m, 2360w, 1598m, 1497s, 1398w, 1358w, 1233s, 1162m, 1104w, 1090w, 1014m, 871w, 833m, 785s, 778s, 735w, 607s, 532m, 408w.
5	$C_{72}H_{52}N_4O_2S_8Zn_2$ (1392.49)	88	>110 dec.	62.11 (62.10)	3.75 (3.76)	4.00 (4.02)	18.50 (18.42)	…	3051w, 2910w, 2851w, 2360m, 2336m, 1611m, 1596m, 1502s, 1440m, 1396m, 1313m, 1227s, 1161m, 1110s, 1068m, 869m, 797s, 775s, 736w, 490w, 475w.
6	$C_{72}H_{52}Cd_2N_4O_2S_8$ (1487.99)	83		58.25 (58.17)	3.50 (3.53)	3.80 (3.77)	17.35 (17.26)	…	3045w, 2962w, 1596m, 1495s, 1393w, 1356w, 1233s, 1161m, 1072w, 1010m, 990m, 960m, 850w, 832m, 777s, 632w, 512w.

Table 2. NMR spectral data for **L^1-L^6** and **1-6**.

Entry	NMR Data (ppm) ^{1}H and ^{13}C	
	^{1}H NMR	**^{13}C NMR**
1 ($CDCl_3$)	1.428 (t; CH_2), 3.225 (q; CH_3), 4.329 (s, CH_2), 5.095 (m; CH_2), 6.618-6.944 (m; Ph), 7.253-7.389 (m; Ph).	9.23 (CH_3), 46.42, 48.72, 56.41 (CH_2), 113.79, 117.07, 119.58, 121.72, 127.33-129.01, 133.01-159.46 (Ph), 210.72, 210.82, 211.04, 211.14 **(-$N^{13}CS_2$)**.
2 (DMSO-d_6)	5.430(d, CH_2), 6.622-7.027, 7.291-7.411 (m; Ph).	46.16, 47.32(CH_2), 113.60-158.51(Ph), 209.07, 209.08, 209.25, 209.27 **(-$N^{13}CS_2$)**.
3 (DMSO-d_6)	4.235 (d, CH_2), 5.479 (s, CH_2), 6.230 (t, Ph), 6.578-6.821, 7.033-7.114, 7.229-7.379 (m; Ph).	46.23, 47.40 (CH_2), 113.57-148.86(Ph), 211.90 **(-$N^{13}CS_2$)**.
4 ($CDCl_3$)	1.142(t, CH_3), 3.142(m, CH_2), 4.737, 5.565, 6.018(s, CH_2), 6.653-7.016, 7.438-7.738, 7.771-8.314(m, Ph).	8.98(CH_3), 45.88(CH_2), 52.47, 53.76, 53.80, 53.88, 56.30, 56.34(CH_2), 113.42, 113.51, 119.48-159.27(Ph), 208.89, 208.92, 208.96, 208.98**(-$N^{13}CS_2$)**.
5 (DMSO-d_6)	4.650(d), 6.046(t) (CH_2), 6.613, 6.693(d), 7.457(t), 7.557(m), 7.830(d), 7.963(dd), 8.145(d) (Ph).	45.71, 46.18(CH_2), 113.44, 119.50, 124.13, 125.56, 125.92, 126.15, 126.51, 127.74, 128.94, 131.64, 133.85, 135.62, 145.17, 148.91 (Ph).
6 (DMSO-d_6)	4.664 (m, CH_2), 5.946 (s, CH_2), 6.188-6.990, 7.406-7.546, 7.703-7.938, 8.152 (m; Ph).	46.20 (CH_2), 113.42-146.35(Ph).

5B.2.2. Host-Guest Reactivity Study (Jobs Plot)

Stock solutions of the binuclear M^{II}dithiocarbamate macrocyclic receptors **1-4** were studied with DMSO solution (1×10^{-5} M). The guest (1,4-dioxane, 4,4'-bipyridine, Piperazine and triethyl amine) solutions (1×10^{-5} M) in DMSO solvent were used to evaluate effect of different guest on macrocyclic receptors. The UV-visible spectrum was taken for each of the different solutions containing a total of 3.0 mL of the receptor and guest species solutions in the following ratios: 3.0:0, 2.5:0.5, 2.0:1.0, 1.5:1.5, 1.0:2.0, 0.5:2.5 and 0.0:3.0. The data was plotted to explore the impact of guest species on receptors.

5B.2.3. *In vitro* cytotoxic study: MTT assay for cell viability/ proliferation

The cell growth inhibition property for the investigated compounds against both the cell lines was determined by MTT assay with some modifications.[4] The binuclear M^{II}dithiocarbamate macrocyclic complexes **1-6**, corresponding metal acetates and Cisplatin were dissolved in DMSO and then diluted with water. The content of DMSO in the resultant solution for each sample was 1%. Cells were seeded in 96-well plates at a density of 1×10^3 cells per well followed by incubation for 24 h. The cells were treated with different concentrations of binuclear M^{II}dithiocarbamate macrocycles under investigation for 6 h against **HEP 3B** and for 14 h **IMR 32** cell lines. Thereafter, the media were removed and the culture was incubated with 20 μL of media containing 5 mg/ml stock solution of MTT in PBS and 60 μL of DMEM for 6 h at 37 °C in 5% CO_2 incubator. The metabolically viable cells leads to the formation of formazan crystals which further dissolved by adding DMSO. As the extent of formazan production is proportional to the number of viable cells, the formazan was estimated by the optical density measurement at 570 nm by ELISA reader (METERTECH-∑960).

5B.3. Results and Discussion

5B.3.1. Syntheses and Characterization

The self-assembly of a discrete supramolecular structure always proceed in competition with polymerization,[5] however, literature reports underline its dependency on the stereo-electronic features of the ligand framework,[6] nature of transition metal centers[7] as well as thermodynamic conditions.[8] The formation of macrocycles is facilitated by the thermodynamic preference even if they are strained to some extent, profiting from enthalphic as well as entropic effects over oligomeric or polymeric species.

The one-pot reaction protocol involving self-assembly of diamine precursor **L^1** or **L^2** with CS_2 and corresponding metal acetates in Et_3N affords access to a series of binuclear M^{II}dithiocarbamate macrocyclic scaffolds [M^{II}_2-μ^2-bis-{(κ^2*S*,*S*-$S_2CN(R)C_6H_4)_2O$}].L **1-6**. The overall synthetic strategy is outlined in Scheme 1. The one-pot synthetic methodology has been utilized extensively by Beers and his coworker to develop self-assembled dithiocarbamate–transition metal macrocycles. Such a methodology involving several chemical operations simultaneously in a single vessel has several distinctive advantages such as it can reduce the purifications of the intermediate compounds, predominantly important with unstable intermediates and may eventually save valuable resources. The green colored binuclear Ni^{II}dithiocarbamate macrocycles (**1, 4**), white colored binuclear Zn^{II}dithiocarbamate macrocycles (**2, 5**) and yellow colored binuclear Cd^{II}dithiocarbamate macrocycles (**3, 6**) exhibit good solubility in common organic solvents. The products isolated appear to be air stable in the solid and in the solution state over a period of time.

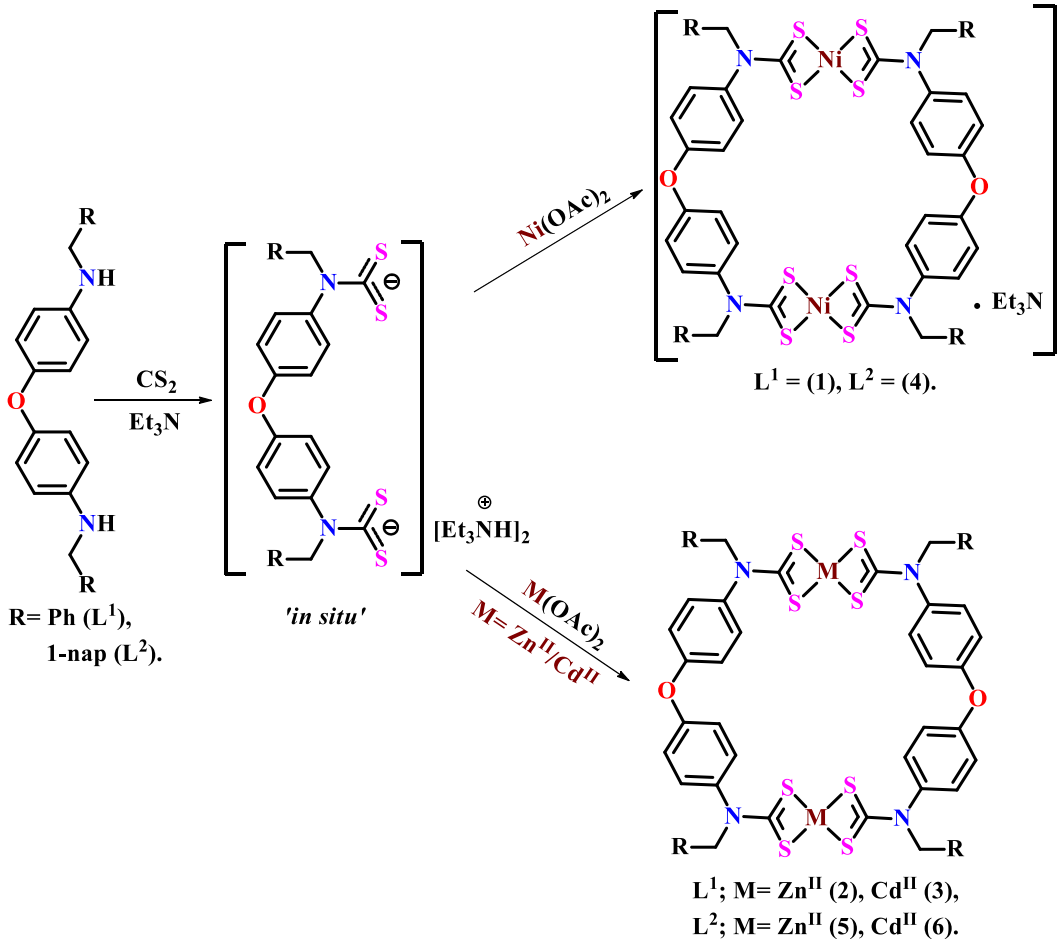

Scheme 1. One-pot synthetic strategy for binuclear M^{II}dithiocarbamate macrocycles **1-6**.

Despite these compounds could not be obtained in the crystalline state, their composition and structures were elucidated by microanalysis, various spectroscopic data and DFT study. The elemental analysis data for binuclear M^{II}dithiocarbamate macrocycles **1-6** are in good agreement with their compositions as per the proposed chemical formula which is mutually supported by subsequent spectroscopic data and thereafter theoretical studies. The characterization data for **1-6** is summarized in the experimental section. Electrospray mass spectrometry (ESMS) in acetonitile solutions confirmed the presence of all dinuclear macrocyclic structures. Binuclear M^{II}dithiocarbamate complexes **1-4** (except **3**) gave m/z peaks at 1279.7, 1213.3 and 1343.3 which correspond to $[M.Et_3N+H]^+$, $[M+Na]^+$ and $[(M-S)+H]^+$ respectively in a positive ion mode. However, complex **3** display m/z peak in a negative ion mode at 1320.5, corresponds to $[M+Cl]^-$ molecular ion. In addition to these peaks, complexes exhibit m/z peaks for expected molecular fragments. In the IR spectra of complexes **1-6,** the absence of ν(N-H) vibration bands (3390-3370 cm^{-1}) and appearance of new bands in the regions 1502-1495 cm^{-1} and 1110-963 cm^{-1}, attributable to characteristic ν(N-CSS) and ν_{assy}(CSS) stretching vibrations, clearly suggest an anisobidentate chelation of the dithiocarbamate ligands.[9] A significant enhancement in the ν(C–N) frequency of the complexes by comparison to that found in free diamine precursors indicates the importance of electron delocalization over coordinated ligand moieties (R = N^+–CS_2^{--}). Notably a strong band at ~ 860 cm^{-1} appeared due to the aromatic ν(C-H) out-of plane bending vibrations, a characteristic feature of para-disubstituted benzene rings.[8] The ν(M-S),[10] occurring in the far-IR region greatly depends on the nature of the metal ion and the ancillary part of ligand. In agreement with the observations made by Sonbati,[10] we have observed medium to weak intensity ν(M-S) bands in the 554-454 cm^{-1} range. All the complexes display characteristic ^1H and ^{13}C NMR signals associated with various molecular sub-units with proper splitting and thus confirming their composition and purity. A significant shifting of the *N*-methylene signals of the complexes, compared to free diamine precursors reinforce the formation of proposed structures as they are most sensitive to any kind of chemical change at amine functionality. The binuclear M^{II}dithiocarbamate macrocycles **1-4** display a set of four downfield resonance in the δ 208.5 to 212.0 ppm range, characteristic of coordinated dithiocarbamates (-$N^{13}CSS$).[11] The appearance of four downfield -$N^{13}CSS$ signals confirm the existence of four non-equivalence dithiocarbamate moieties in the solution

state. We could not detect the -N^{13}CSS signals for complexes **5** and **6** even after an increased number of scans mainly due to their inadequate solubility. The relatively poor solubility of complexes **5** and **6** could be due to the presence of several aromatic and dithiocarbamate moieties leading to a massive number of intermolecular non-covalent interactions such as CH-π, π-π and M...S interactions. The appearance of sharp signals with proper splitting patters in the NMR spectra of binuclear complexes **1-6** and their good solubility in common organic solvents give strong evidence for the formation of discrete macrocyclic complexes and ruled out the possibility of formation of oligomers or coordination polymers. Normally, due to the large size of the structure and exhaustive conformational mobility within the polymetallic assemblies, multiple signals or broadening of NMR signals are seen for oligomers or coordination polymers.

5B.3.2. Optical Properties

UV-visible absorption, emission and transmittance: The UV-visible absorption and emission spectra of ligand precursors **L^1**, **L^2** and binuclear M^{II}dithiocarbamate complexes **1-6** were measured at room temperature from 10^{-5} M DMSO solution samples. The UV-visible absorption and emission spectra of the investigated compounds are provided in annexure the whereas pertinent results are summarized in Table 1.

Table 1. UV–visible absorption, emission and optical band gap data for ligand precursors [a] **L^1, L^2** and binuclear M^{II}dithiocarbamate complexes **1-6**.

Entry	UV-Visible Absorption Spectral data λ_{max} nm (ε, L mol^{-1} cm^{-1})	Emission Spectral data λ_{em} nm (Intensity)	λ_{ex} (nm)	Band Gap Ea (eV)
L^1	253 (38616) π→π* (phenyl) 307 (17366) n→π* (amine)	360 (36) π*→n (dtc)	307	2.1677
L^2	253 (35066) π→π* (phenyl) 285 (29934) π→π* (amine)	346 (7) π*→π (phenyl) 497 (8) π*→π (phenyl)	284	2.2897
1	261 (56324) π→π* (phenyl) 332 (57565) n→π* (N–C=S) 388sh (19509) charge transfer	308 (193) π*→π (phenyl) 372(1000) π*→π (phenyl) 536(321) π*→π (phenyl)	261	2.0521
2	267(58322) π→π* (phenyl)	328(36) π*→π (phenyl) 371(211) π*→π (phenyl)	267	2.6184
3	282 (52417) π→π* (phenyl) 438 (21498) charge transfer	416 (105) π*→π (phenyl) 437 (114) br, π*→π (phenyl)	282	2.3355
4	286 (51860) π→π* (phenyl) 326 (43096) n→π* (N–C=S) 409sh (8102) charge transfer	374 (165) π*→ n (dtc) 533 (517) π*→ n (dtc) 586 (355) π*→ n (dtc) 640 (269) π*→ n (overtone)	326	2.3070
5	271 (45387) π→π* (phenyl)	371 (697) π*→π (phenyl)	271	2.5052
6	265(15361) π→π* (phenyl) 478(31961) charge transfer	330 (775) π*→π (phenyl)	265	2.3013

a: For comparison, UV-visible absorption, emission and transmittance data retrieved from reference 19, 22.

The UV-visible absorption spectra of **L^1-L^2** exhibit two prominent bands at shorter wavelengths ~250 nm and ~280 nm, attributable to π→π* (phenyl) and π→π* (amine) transitions, respectively.[12] All the binuclear complexes show two principal bands at 261-286 nm region and at 388-478 nm region, attributable to π→π* (phenyl) and charge transfer transitions, respectively, except Zn(II) complexes **2** and **5** which exhibit featureless electronic spectra presenting a broad absorption at ~270 nm. The diamagnetisms along with UV-visible absorption bands suggest square planar/distorted square planar environment around Ni^{II} and tetrahedral/distorted tetrahedral environment around Zn^{II}/Cd^{II} centers in their respective complexes.[12]

On the other hand, fluorescence study evidently depicted the enhancement in fluorescence property of binuclear M^{II}dithiocarbamate macrocyclic complexes **1-6**, compared to their respective ligand precursors **L^1** and **L^2**. This can be expected due to an efficient delocalization of π-electrons and conformational rigidity acquire by the macrocyclic molecular framework, reducing the nonradiative decay. All the complexes 1-6 exhibit maximum fluorescence emissions at 372, 371, 437, 533, 371 and 330 nm upon excitation at 261, 267, 282, 326, 271 and 265 nm with concomitant Stokes shifts of 111, 96, 155, 207, 100 ≈ 65 nm, respectively. Notably, among all the binuclear M^{II}dithiocarbamate macrocycles, complex **1** bearing Ni^{II} center exhibit the maximum fluorescence property which may be attributed to the reduction of photoinduced electron transfer process on complex formation.[13] The emission spectra of majority of the complexes displayed similar patterns, i.e. two or more kinds of fluorescence emission bands are appearing by the excitation of single absorption bands (in any case, shoulder is appearing). Such a trend of fluorescence spectra and concomitant bathochromic shifts of intramolecular charge-transfer emissions is consistent with previous reports on transition metal dithiocarbamate complexes.[14] It appears from the literature that the photoinduced electron transfer processes, hence fluorescence properties of the compounds is greatly affected by the molecular arrangements, conformational stiffness of the fluorophore, non-covalent interactions.[15]

Furthermore, binuclear M^{II}dithiocarbamate complexes **1–6** were investigated for their potential optical behavior towards wide band-gap semiconducting nature using UV–visible transmittance measurements. The values of optical energy band gaps and their nature were derived from electronic excitation from the valence band to conduction band as described elsewhere.[8] The optical absorption coefficients, α; were

obtained from the transmittance spectrum of complexes **1–6** using the formula: $\alpha = \frac{1}{d}\ln[\frac{1}{T}]$, where, d is the thickness of the samples and T is the transmittance. The relation between the absorption coefficients (α) and the incident photon energy (hν) can be determined using the well known Davis and Mott equation,[16] $\alpha h\nu = [D(h\nu - Eg)]^{\gamma}$ where, constant D is the edge width parameter. The exponent γ depends on the type of transition occur in the material. In order to determine optical band gap energies (*Eg*) for binuclear M^{II}dithiocarbamate macrocycles **1-6**, we have applied the models for both direct and indirect transitions. For this, the $(\alpha h\nu)^2$ (direct transition) and $(\alpha h\nu)^{1/2}$ (indirect transitions) versus hν were plotted for each compound. The values of *Eg* obtained for an entire group of compounds **1-6** by extrapolating the linear part of the Tauc plot[17] (with c = 1/2) suggest the absorption in these samples corresponds to a direct energy gap. The band gap energy for all the complexes falls in 2.1-2.6 eV range and exhibits a feature of direct band gap semiconductor.[8] Expectedly the *Eg* for all the complexes (except 1) are higher than their corresponding diamine precursors as polyamines are well known conducting materials with lower band gap energies.

5B.3.3. Thermogravimetric Studies for 1-6

All the binuclear M^{II}dithiocarbamate macrocycles **1-6** were studied for their thermal behavior. The thermogravimetric study for **1-6** was performed at a heating rate of 10 °C /min under N_2 atmosphere from room temperature to 550 °C. The TGA/DTA plots and thermal analysis data are given in annexure.

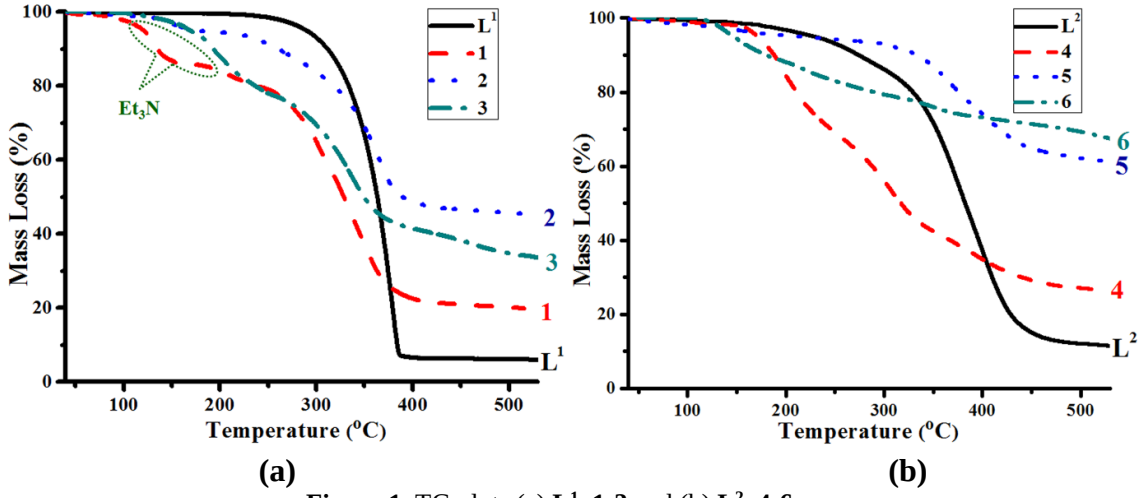

Figure 1. TG plots (a) **L**[1], **1-3** and (b) **L**[2], **4-6**.

Notably, all the dithiocarbamate complexes **1-6** showed a multistage thermal degradation pattern due to the elimination of different molecular fragments, evidence

by TG curves (Figure 1) which are indeed accompanied by corresponding peaks on DTG curves. This is consistent with the degradation patterns showed by several transition metal dithiocarbamate complexes.[18] Although, the thermal degradation of Zn^{II}/Cd^{II} complexes is continued at 550 °C, however, Ni^{II} complexes **1** and **4** gave a stable residual mass of 20.1% and 29.5 % which correspond to NiS (calc. 14.18 % for **1** and 12.26 % for **4**) plus char, respectively. Reportedly the size and shape of the metal sulfide nanoparticles greatly depend on the nature of organic moiety present in metal dithiocarbamate complexes[19] which consecutively affect the fundamental properties such as optical, electrical and mechanical.[20] The thermogravimetric analysis indicates the suitability complexes **1** and **4** as single source precursors for the synthesis of metal sulphide nano particles and thin films[21] which adds further merit to this work. Moreover, the binuclear Ni^{II}dithiocarbamate macrocycles **1** display first weight loss of 8.4% in the temperature of 100-150°C which can be assigned to the loss of one triethyl amine molecule (calcd. 7.8%). The loss of triethyl amine fragment at much higher temperature than its boiling point confirms the association of **1** and Et_3N. Earlier, the microanalysis and NMR data clearly evident the association of Et_3N molecules with both of the Ni^{II}dithiocarbamate macrocycles **1** and **4**, however the TG curve of 4 could not display the loss of Et_3N molecule distinctly due to continuous mass loss.

5B.3.4. Host-Guest Reactivity Study (Jobs Plot)

The interaction of Et_3N molecules with compounds **1** and **4** in 1:1 stoichiometry has been clearly revealed by microanalysis, NMR later by thermogravimetric analysis. This has encouraged us to explore the host-guest binding ability of some of these macrocyclic complexes towards a number of guest species viz. 1,4-dioxane, 4,4'-bipyridine, piperazine and triethyl amine by using UV-vis absorption spectrophotometry.

Job plot experiments revealed that **1-4** forms host–guest complexes in 1:1, 1:2 and 2:1 stoichiometries, depending on the relative sizes of the hosts-guests and their electronic nature (annexure). Evidently, the binding of bidentate guest species outside the receptor cavity is unaffected by the size of the macrocyclic cavities. For instance, in spite of the large macrocyclic cavity sizes of receptors 1-4, they fail to accommodate all the bidentate guests (*vide supra*) to form 1:1 inclusion complex, instead receptor 1 predominantly forms 1:2 complex while receptor 2 forms 2:1 complex exclusively with all the bidentate guests, whereas receptors 3 and 4 forms such a complex only with

piperazine and 4,4'-bipyridine, respectively. The binding behavior of these bidentate guests is consistent with the behavior of terephthalate and isonicotinate with ditopic dinuclear zinc(II) dtc macrocyclic receptors.[11c] The host–guest binding stoichiometry for receptor **4** with bidentate guests 1,4-dioxane ~ (2.9 × 4.8 A) and piperazine ~(4.73 × 4.87 A) was found to be 1:1, indicating the formation of intramolecular inclusion complexes (Figure 2) in Job plot experiments. Although, the size of this host is much larger (12.2 × 6.1 A) than the guest species receptors **4,** however the formation of such inclusion complexes may be associated with the flexibility of –[Ar-O-Ar]- spacer group causes variation in the transannular Ni–Ni distance and thereby the cavity size and shape of the receptor. Moreover, the unique bowl shaped architecture adopted by this receptor **4** (Figure 2) may allow small sized bidentate guests to enter into the molecular cavity (bowl) and forms 1:1 complex, whereas bulkier 4,4'-bipyridine guest failed to form such complex, instead it showed 2:1 complex. All the receptors form 1:2 complexes with Et_3N, except receptor **1** suggesting cavity size independent binding of this guest with receptors. The presence of M^{II} dithiocarbamate Lewis acid center into a cyclic framework structure allows the efficient interaction with Lewis base guests, probably converting the square planar Ni^{II} dithiocarbamate and tetrahedral Zn^{II}/Cd^{II} dithiocarbamate moiety into a five-coordinate square pyramidal complex, respectively.[22]

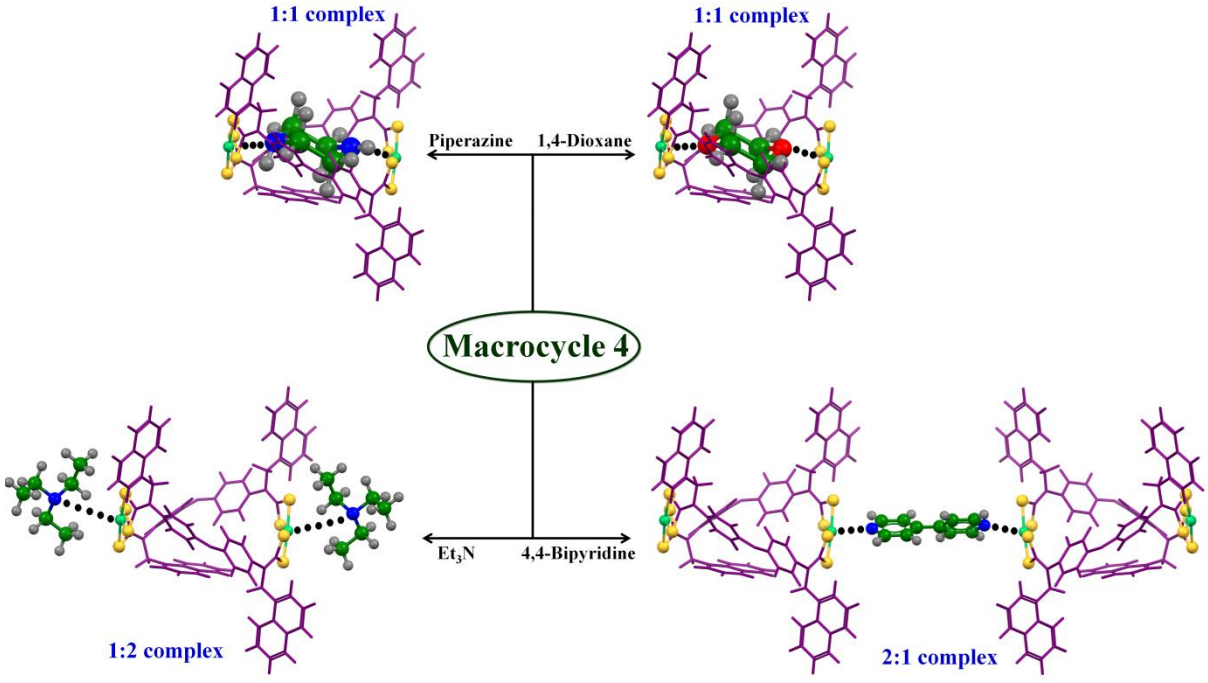

Figure 2. A representation of binding modes of receptor **4** with various guests.

5B.3.5. Computational Investigations

To get a better understanding of the spectroscopic results and to establish structure-property correlation, a DFT level calculation has been performed on diamine precursors **L^1-L^2** and binuclear M^{II}dithiocarbamate macrocyclic complexes **1-6**. Such calculations have been widely used in recent years due to its ability to provide reasonably good results for huge molecular structures, including transition metal complexes.[23] All the calculations were performed using the Gaussian 03 program suite[24] and molecular orbitals were generated by GaussView 3.0 program. Full geometry optimizations of diamine precursors **L^1-L^2** and complexes **1-6** were performed using density functional theory (DFT) at B3LYP/6-31G (d, p) and B3LYP/LanL2DZ basis sets, respectively. Such type of basis set has been used with good success in a number of studies involving similar species, having a good agreement with experimental results.[23] An optimized geometry for the minimum energy conformation of **L^1-L^2** and binuclear complexes **1-6** are given in Figure 3 whereas structural parameters are summarized in Table 2.

Table 2. Summary of DFT study performed on **L^1**, **L^2** at the DFT B3LYP/ 6-31G (d, p) level and binuclear M^{II}dithiocarbamate complexes **1-6** at the DFT B3LYP/LanL2DZ level

Entry	Energy of Optimized Geometry (Hartree)	Coordination Geometry	Transannular M···M Distance (Å)	E_{HOMO}, E_{LUMO} (eV)	$E_{HOMO-LUMO}$ (eV)	λ_{max} cal. (exp) nm
L^1	-1189.9755	…	…	-4.7782 -0.1967	4.5814	271 (277)
L^2	-1497.2624	…	…	-4.8478 -1.1048	3.7430	331 (313)
1	-6054.1712	distorted square planar	9.959	-5.4797 -1.8023	3.6774	237 (233)
2	-5846.7443	distorted tetrahedral	10.402	-5.8823 -1.0795	4.8028	258 (267)
3	-5811.6669	distorted tetrahedral	10.494	-5.7836 -1.0719	4.7118	263 (281)
4	-6668.6825	distorted square planar	12.205	- 5.7251 - 2.2602	3.4649	358 (337)
5	-6461.2899	distorted tetrahedral	10.476	- 5.8285 - 1.2909	4.5376	273 (260)
6	-6426.1713	Intermediate geometry between tetrahedral and square planar	13.682	- 5.5921 - 1.8183	3.7738	329 (350)

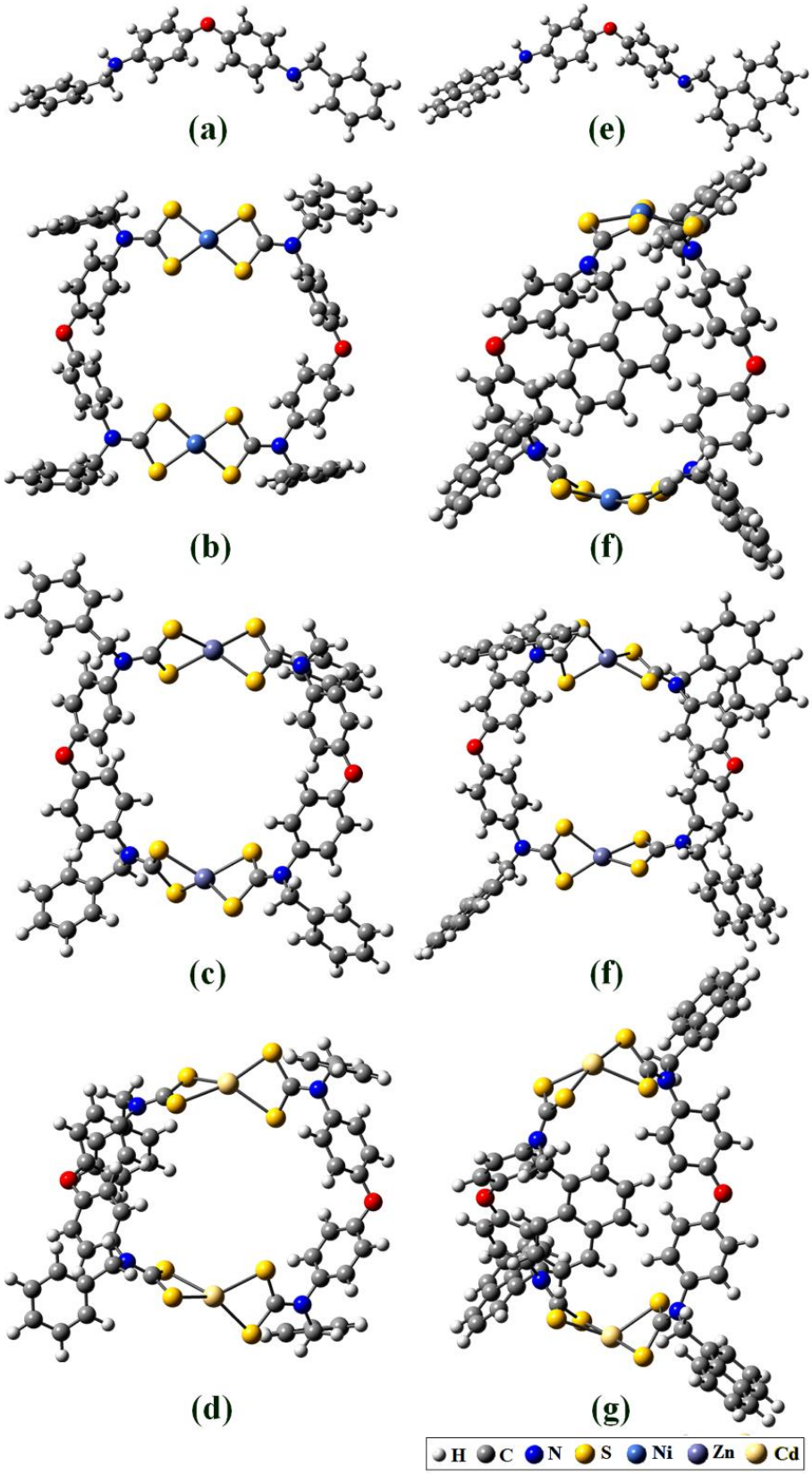

Figure 3. An optimized geometry for the minimum energy conformation of (a) $\mathbf{L^1}$, (b) **1**, (c) **2**, (d) **3**, (e) $\mathbf{L^2}$, (f) **4**, (g) **5** and (h) **6**.

For binuclear M^{II}dithiocarbamate complexes **1-6**, optimized geometries clearly suggest that each dithiocarbamate ligands bridge two metal centers *via* chelating

dithiocarbamate moieties, resulting in the formation of binuclear macrocyclic architectures. The optimized structures (Figure 3) clearly suggest the distorted square planar coordination geometry around both the Ni^{II} nucleus in binuclear dithiocarbamate complexes **1**, **4**; distorted tetrahedral coordination geometry around both the Zn^{II} and Cd^{II} centers in their corresponding dithiocarbamate complexes **2-3**, **5-6**. The study also points out nearly coplanar macrocyclic ring as minimum energy conformation for binuclear M^{II}dithiocarbamate complexes **1-3** and **5**. Among four *N*-substituents, three are projected towards either side of the molecular plane and one is leant to the opposite side of the molecular plane in 1-3, while in case of **5**, each set of two substituents is oriented towards either side of the molecular plane. Interestingly, complexes **4** and **6** exhibit bowl shaped molecular architectures (Figure 4) as minimum energy conformation. Among the four 1-naphthylmethyl groups, two are projected towards upper side, one is projected below and the fourth one is arranged parallel to the molecular plane to compensate stereo-electronic repulsion.

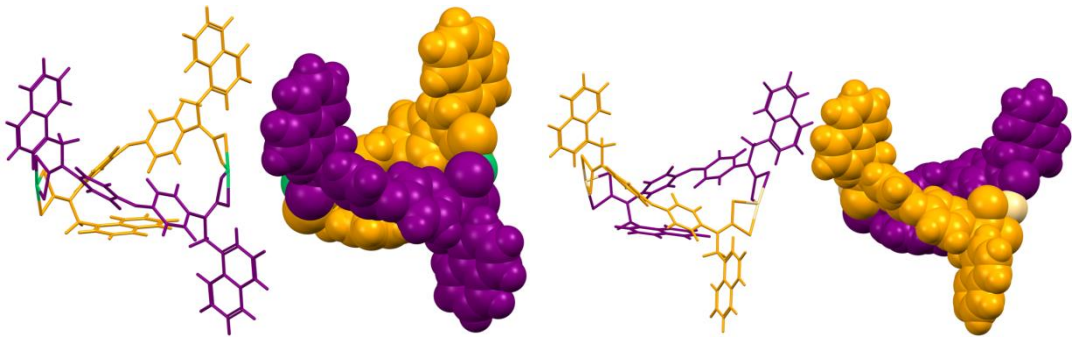

(a) **(b)**

Figure 4. An illustration of a bowl shaped molecular architecture for (a) **4** and (b) **6** in capped stick and spacefill models.

The dithiocarbamate functionalities are most vulnerable to any change in the electronic environment induced by the aromatic substituents as they are present in the close vicinity. This could be the basis for magnetic non-equivalence of dithiocarbamate moieties present in a molecular framework which is also experimentally supported by more than one ^{13}C NMR signals for $-N^{13}CSS$ moiety. The selected structural parameters for the optimized geometries of **1-6** are summarized in Table 3. It appears from the optimized geometries that there is a gradual increase in the bond lengths associated with M^{II}dithiocarbamate moieties from Ni-Zn-Cd in all the complexes 1-6 and this trend is indeed unaffected by various N-substituents; however a significant effect of these substituents can be seen on C—O—C bond angles. For instance, gradual

decrease in C-O-C bond angle is appeared for complexes Ni-Zn-Cd bearing N-benzyl substituents whereas reverse trend is observed for those bearing *N*-(1-naphthyl methyl) substituents.

Table 3. Selected geometrical parameters obtained from the optimized geometry of complex **1-6**.

Selected Bond	Bond lengths (Å)	Selected Bonds	Bond angles (°)
		L^1	
N—C	1.400-1.457	C—O—C	119.73
		L^2	
N—C	1.402-1.454	C—O—C	119.74
		1	
N—C	1.346-1.348	S—Ni—S (chelate)	78.227-78.281
C—S	1.726-1.734	S—Ni—S (trans S)	174.98-176.64
Ni—S	2.266-2.293	C—O—C	117.91-117.98
		2	
N—C	1.349	S—Zn—S (chelate)	75.75-75.80
C—S	1.738-1.749	S—Zn—S (trans S)	118.02-118.58, 129.79-133.31
Zn—S	2.442-2.455	C—O—C	117.68
		3	
N—C	1.352	S—Cd—S (chelate)	70.36-70.39
C—S	1.738-1.750	S—Cd—S (trans S)	119.62-137.83
Cd—S	2.619-2.639	C—O—C	117.65
		4	
N—C	1.347-1.357	S—Ni—S (chelate)	78.21-78.38
C—S	1.727-1.739	S—Ni—S (trans S)	156.83-175.42
Ni—S	2.274-2.283	C—O—C	118.99, 120.26
		5	
N—C	1.349, 1.353	S—Zn—S (chelate)	75.73-75.77
C—S	1.738-1.749	S—Zn—S (trans S)	117.77-134.63
Zn—S	2.443-2.452	C—O—C	118.11, 118.15
		6	
N—C	1.352, 1.360	S—Cd—S (chelate)	69.40-69.80
C—S	1.737-1.751	S—Cd—S (trans S)	103.06-174.71
Cd—S	2.632-2.652	C—O—C	125.07, 122.75

Table 4. Selected geometrical parameters obtained from X-ray structures.[25]

Selected Bond	Bond lengths (Å)	Selected Bonds	Bond angles (°)
		Binuclear Ni^{II}dithiocarbamate complex	
N—C	1.318-1.326	S—Ni—S (chelate)	79.39-79.47
C—S	1.710-1.722	S—Ni—S (trans S)	176.47-179.04
Ni—S	2.200-2.208	coordination geometry	square planar
		Binuclear Zn^{II}dithiocarbamate complex	
N—C	1.340-1.361	S—Zn—S (chelate)	77.23-79.01
C—S	1.683-1.801	S—Zn—S (trans S)	117.44-136.16
Zn—S	2.348-2.406	coordination geometry	Distorted tetrahedral

Further, structural parameters (Table 3) obtained from optimized geometries were compared with those obtained from X-ray study (Table 4) of closely related compounds.[25] It appears that in case of M^{II}dithiocarbamate complexes **1-6**, C-S, M-S, N-CS_2 bond distances and S—M—S (chelate), S—M—S (trans) angles are somewhat overestimated, compared to the experimental results reported. This slight disparity in

the structural parameters could be explained by the mutual effect of differential stereoelectronic factors and the existence of extensive non-covalent interactions.[25]

The molecular electrostatic potential (MESP) of any chemical species provides valuable information about electronic environment of the molecule, useful for the prediction of its properties and potential sites for reactivity, including biological systems.[26] The localization of slight negative potential around respective metal centers in complexes **1**-**3** and **5** whereas as positive potential around metal centers in bowl shaped complexes **4** and **6** could be clearly revealed from mapping of electrostatic potential surface. This generates a scope for fine tuning of reactivity of any ditopic receptors bearing identical spacer moiety, through modification at metal ion and aromatic substituents resulting in varied cavity size and electronic environment for effective interaction with various guest molecules including biomolecules.

Moreover, an investigation of frontier molecular orbitals becomes essential for speculation of the potential reactivity of the molecule due to their vital contribution in the photo-physical properties, especially localization and the HOMO–LUMO energy gap.[27] The calculated HOMO-LUMO energy gaps (Isovalue = 0.02) for ligand precursor $\mathbf{L^1}$, $\mathbf{L^2}$ and binuclear M^{II}dithiocarbamate complexes **1**-**6** are given in Table 2 and their localization is illustrated in Figure 5.

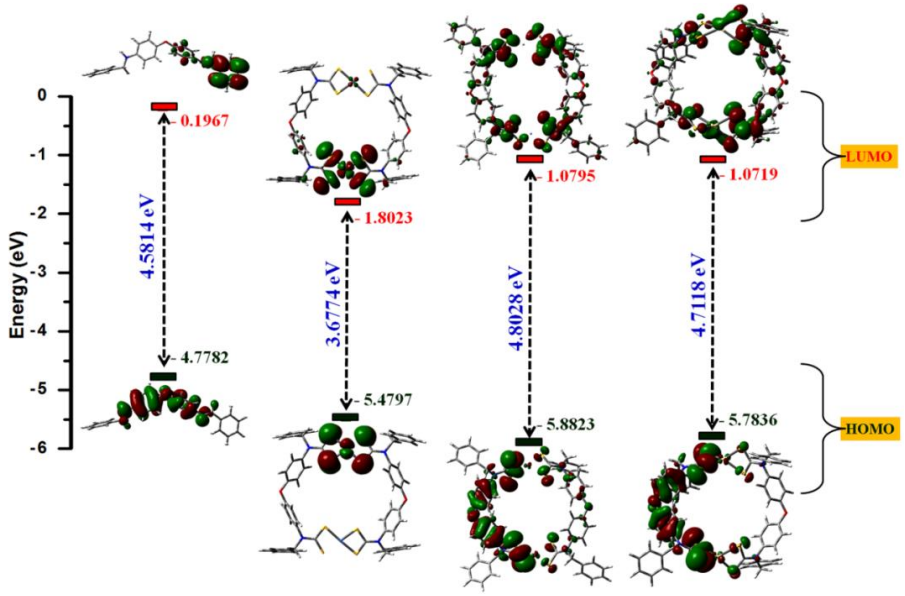

(a)

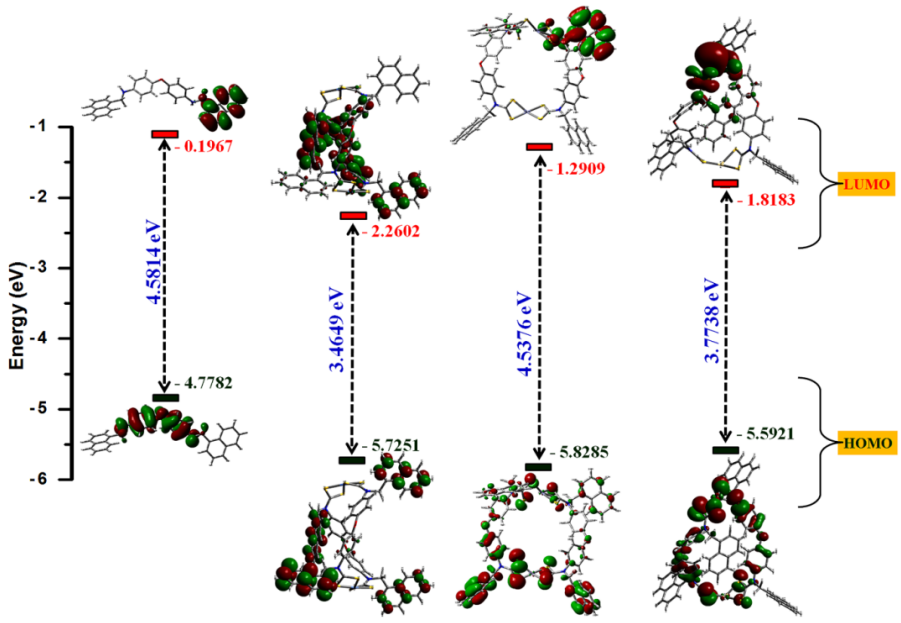

(b)

Figure 5. Frontier molecular orbitals (Isovalue= 0.02) for (a) $\mathbf{L^1}$ and **1-3**, (b) $\mathbf{L^2}$ and **4-6.**

It may be noted that the delocalization of LUMO (Figure 5b) in complex **4** over ethereal phenyl rings, coordinated dithiocarbamate functionality and one *N*-(1-naphthylmethyl) moiety, forming bowl shaped molecular framework, enhancing the Lewis acidic character of this cavity and hence complex **4** is exclusively involve in formation of 1:1 host-guest inclusion complex with bidentate guests (*vide supra*). The HOMO-LUMO energy differences for the Ni^{II}dithiocarbamates **1** (3.6774 eV) and **4** (3.4649 eV) are significantly lower compared to their Zn^{II} and Cd^{II} analogues. The substitution of *N*-benzyl substituents from **1-3** by *N*-(1-naphthylmethyl) in **4-6** causes remarkable decreases in HOMO-LUMO energy gaps due to extended conjugation. Interestingly, the HOMO–LUMO energy gaps for bimetallic dithiocarbamate complexes **1-6** is found in the range 3.4649-4.7118 eV; which are significantly higher than the optical band gaps determined experimentally by using UV-visible transmittance measurements in the solid state. This is obvious because massive numbers of non-covalent interactions can be expected in solid state, causing lowering in the band gaps. Thus, it adds further merits to this class of compounds towards potential applicability as semiconducting materials. λ_{max} values (Table 2) determined experimentally by means of UV-visible absorptions for complexes **1-6** are comparable with HOMO-LUMO gaps obtained by computational study which validate the computational investigations.

5B.3.6. *In Vitro* Cytotoxic Activity

An excellent cytotoxic activity[5] of diamine precursors **L^1** and **L^2** has inspired us to use these compounds further for structural modification in search of better potency. Literature evidences a wide range of macrocyclic natural product and their synthetic derivatives have long been clinically used because of the high degree of potency as well as selectivity achieved by these scaffolds.[28] Despite of metal based macrocyclic complexes widely studied in supramolecular chemistry, especially host-guest reactivity study, [5] this structural class is surprisingly underexploited in medicinal chemistry. Hence, it was pertinent to investigate binuclear M^{II}dithiocarbamate macrocyclic scaffolds **1-6** for their potential anticancer activity by the MTT assay[4] against the malignant human cancer cell lines **HEP 3B** (Hepatoma) and **IMR 32** (Neuroblastoma) and compare their cyctotoxicity with clinically used antineoplastic drug cisplatin. The IC_{50} values shown in Table 5 represent 50 % inhibition concentration against the malignant tumor cell lines were obtained after treatment of M^{II}dithiocarbamate macrocycles for 6 h with **HEP 3B** and 14 h with **IMR 32** cells. (Table 5, Figure 6)

Table 5. *In vitro* cytotoxicity IC_{50} (μM) by MTT assay for entry **1-12** against **HEP 3B** and **IMR 32** cancer cell lines.

Entry	Compound	Antitumor activity (IC_{50} values) μM (1mL) ±SE	
		HEP 3B	IMR 32
1	1	39.27±0.25	35.15±1.06
2	2	58.11±0.24	54.94±1.89
3	3	58.35±0.21	51.71±2.43
4	4	42.07±0.18	40.26±1.65
5	5	66.51±0.18	42.80±0.25
6	6	51.10±0.12	37.13±0.18
7	$Ni(OAc)_2.4H_2O$	457.92±1.21	342.79±15.99
8	$Zn(OAc)_2.2H_2O$	302.52±1.46	192.26±7.61
9	$(Cd(OAc)_2.2H_2O$	195.66±1.24	153.45±9.00
10	Cisplatin	74.62±1.27	61.90±5.19

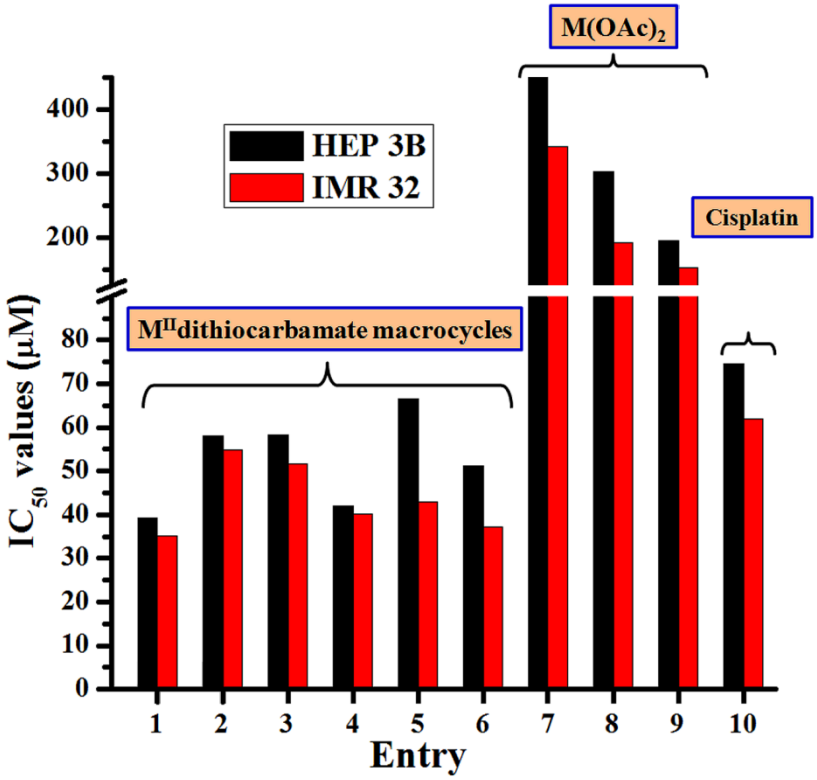

Figure 6. *In vitro* cytotoxicity *i.e.* IC_{50} for compound **1-12** against **HEP 3B** and **IMR 32** cancer cell lines

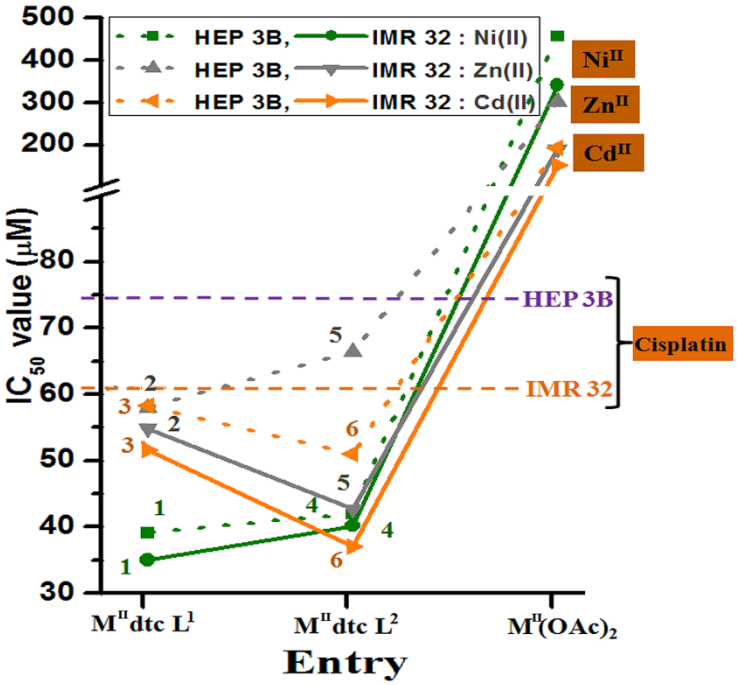

Figure 7. Effect of the change in **'*R* groups'** and ***'M centers'*** towards cytotoxicity against **HEP 3B** and **IMR 32** cancer cell lines.

The binuclear M^{II}dithiocarbamate complexes follows cytotoxicity trends as **1>4>6>2>3>5** against **HEP 3B** and **1>6>4>5>3>2** against **IMR 32** cell lines. The differential reactivity profile and hence potency of **1-6** against **HEP 3B** and **IMR 32** cell lines is mainly associated with unique molecular conformation adopted by the

macrocyclic scaffolds. (Figure 7) The extremely lower potency of metal salts is associated with their ionic nature which become the barrier for the membrane transportation and hence, for the resultant cytotoxic activity. Interestingly, the cytotoxicity trend observed in corresponding metal acetates is almost reversed in their binuclear M^{II}dithiocarbamate macrocycle. For instance, least active $Ni^{II}(OAc)_2$ (457.92±1.21 μM against **HEP 3B** and 342.79±15.99 μM against **IMR 32**) lead to the binuclear macrocycle **1** with optimum cytotoxic activity. The higher potency of all the complexes **1-6** is probably due to the predominant reactivity of chelated dithiocarbamate moiety in biological systems. Furthermore, comparison of the IC_{50} values of screened binuclear macrocycles with the clinically used antineoplastic drug cisplatin clearly underlines the greater potency against both the cancer cell lines, more than two folds in some cases.

In recent days, theoretical calculation is a one of the robust tool used to study structure-activity relationship (SAR)[29] which offers structural and stereo-electronic parameters, useful to get mechanistic insights into the transport of the compound across the cell membranes and possible interactions with biological macromolecules. The surface potential of the molecule is also crucial suggesting the potential sites for non-covalent interactions for instance, hydrogen bonding with biological receptors resulting into the effective cellular membrane transportation.

The cytotoxicity of binuclear M^{II}dithiocarbamate macrocycles **1**-**6** (except **3**) against **IMR 32** appeares to be increases with increase in energy of HOMO. Further the cytotoxicity of **1-6** against **HEP 3B** appears to be increasing with a decrease in the partial charge at sulfur atom suggesting the possible interactions with various nucleophilic moieties present in biological receptors. It appears that binuclear Ni^{II}dithiocarbamate macrocycle **1** with highest HOMO energy (-5.4797 eV), lowest HOMO-LUMO energy difference (3.6774 eV) and least charge on sulfur atoms (-0.191 to -0.226 e.u.) exhibits optimum cytotoxicity among all the binuclear M^{II}dithiocarbamate macrocycles and suggests its higher reactivity in the biological conditions leading to the enhanced potency. The better cytotoxicity of binuclear dithiocarbamate macrocyclic complexes would be due to their accessibility for transchelation reactions with biomolecules and transmetallation reaction with metal ions present at the site of action which alters the hard/soft properties, the

lipophilic/hydrophilic balance of the resulting complexes and help to permeate the cellular membrane.

Although, detailed mode(s) of action for antitumor activity of transition metal dithiocarbamate complexes at molecular level is yet to be completely explored, reports suggest that DNA could be the probable target for the cytotoxic activity[30] as these compounds can affect the primary structure of DNA and induces a complexed, prolonged and variable response in cells which may lead to cell death via regulated apoptosis or necrosis.[31] Further reports suggest that the antitumor activity of dithiocarbamates can be achieved through antiangio-genesis effects, inhibition of numerous metalloenzymes and NF-KB-related gene-expression and modulation of cellular metabolism, which lead to tissue damage.[32] The anticancer potential of nickel complexes reportedly attained by the interaction with DNA and some DNA-binding proteins.[33] The decomposition and metabolic products of a dithiocarbamate complexes in vivo, *ca* free dithiocarbamate moieties, CS_2 are reportedly able to arrest the cell proliferation.[34] Thus it may be anticipated that the observed cytotoxic effects of binuclear M^{II}dithiocarbamate complexes involves all these processes wherein the balance among the processes and their outcomes may differ from one cell type to another and among different organisms.

5B.4. Conclusions

In conclusion, a series of bimetallic dithiocarbamate macrocyclic complexes $[M^{II}_2$-μ^2-bis-{(κ^2S,S-$S_2CN(R)C_6H_4)_2O$}].L (**1-6**) can be efficiently synthesized in a one-pot self-assembling process involving 4,4'-bis(arylmethylamino)diphenyl ether precursors $\mathbf{L^1}$ or $\mathbf{L^2}$, CS_2 and Ni(II), Zn(II) or Cd(II) metal ion. All the complexes exhibit fluorescent property and maximum fluorescence intensity is recorded for binuclear Ni^{II}dithiocarbamate macrocycles complex **1.** UV–visible transmittance measurement evidences the wide band-gap semiconducting behaviour of **1-6**. The thermogravimetric analysis indicates the suitability complexes **1** and **4** as single source precursors for the synthesis of metal sulfide nano particles and thin films. Interestingly, Job plot experiments clearly reveals the ability of macrocycle **4** to form intramolecular 1:1 host–guest inclusion complex with bidentate guests 1,4-dioxane and piperazine. Computational investigations performed on the model compounds reinforced the experimental outcomes and provides valuable information about frontier molecular

orbitals. The enhanced cytotoxic activities of these macrocyclic scaffolds **1-6** against human cancer HEP 3B and IMR 32 cells, as compared to cisplatin, a well known antineoplastic drug makes these compounds biologically significant. Thus, the current study projects an efficient approach to enhance the antiproliferative activity via self assembly process and provides a guideline for the development of a class of compounds having high potency against the human cancer cell lines. Further studies to evaluate the cell viability, membrane and chromosomal damage, cell-cycle analysis and morphological changes in the treated human cancer cells by macrocyclic scaffolds **1-6** towards are underway.

5B.5. References

1. (a) Fujita, M. *Chem. Soc. Rev.* **1998**, *27*, 417. (b) Hawthorne, M. F.; Zheng, Z. *Acc. Chem. Res.* **1997**, *30*, 267. (c) Beer, P. D.; Gale, P. A. *Angew. Chem., Int. Ed.* **2001**, *40*, 486. (d) Chen, B.; Xiang, S.; Qian, G. *Acc. Chem. Res.* **2010**, *43*, 1115. (e) Uppadine, L. H.; Weeks, J. M.; Beer, P. D. *J. Chem. Soc., Dalton Trans.* **2001**, 3367. (g) Wong, W. W. H.; Cookson, J.; Evans, E. A. L.; McInnes, E. J. L.; Wolowska, J.; Maher, J. P.; Bishop, P.; Beer, P. D. *Chem. Commun*. **2005**, 2214. (h) Beer, P. D.; Berry, N. G.; Drew, M. G. B.; Fox, O. D.; Padilla-Tosta, M. E.; Patell, S. *Chem. Commun.* **2001**, 199.
2. (a) W.-Ely, J. D. E. T.; Solanki, D.; Hogarth, G. *Eur. J. Inorg. Chem.*, **2005**, 4027. (b) Cookson, J.; Beer, P. D. *J. Chem. Soc. Dalton Trans*. **2007**, 1459.(c) Beer, P. D.; Berry, N. Drew, M. G. B.; Fox, O. D.; P.-Tosta, M. E.; Patell, S. *Chem. Commun.* **2001**, 199. (d) Wong, W. W. H.; Curiel, D.; Cowley, A. R.; Beer, P. D. *Dalton Trans.* **2005**, 359.
3. Singh, V. K.; Kadu, R.; Roy, H. *Eur. J. Med. Chem.* **2014**, *74*, 552.
4. Manosroi, J.; Dhumtanom, P.; Manosroi, A. *Cancer Lett.* **2006**, *235*, 114.
5. Ercolani, G. *J. Phys. Chem. B* **2003**, *107*, 5052.
6. Leininger, S.; Olenyuk, B.; Stang, P. *Chem. Rev.* **2000**, *100*, 853.
7. Jones, C. J. *Chem. Soc. Rev.* **1998**, *27*, 289.
8. Kadu, R.; Singh, V. K.; Verma, S. K.; Raghavaiah, P.; Shaikh M. M. *J Mol. Struct*. **2013**, *1033*, 298.
9. (a) Chauhan, R.; Trivedi, M.; Singh, J.; Molloy, K. C.; K.-Köhn, G.; Mulik, U. P.; Amalnerkar, D. P.; Kumar, A. Inorg. Chim. Acta **2014**, *415*, 69. (b) Reyes-

Martínez, R.; Mejia-Huicochea, R.; G.-Alvarez, J. A.; Höpfl, H.; Tlahuext, H. *ARKIVOC* **2008**, *v*, 19.

10. (a) Siddiqi, K. S.; Nami, S. A. A.; Lutfullah, Chebude,Y. *J. Braz. Chem. Soc.*, **2006**, *17*, 107. (b) Bensebaa, F.; Zhou, Y.; Brolo, A. G.; Irish, D. E.; Deslandes, Y.; Kruus, E.; Ellis, T. H.; *Spectrochim. Acta* **1999**, *55A*, 1229. (c) E.-Sonbati, A. Z.; *Synth. React. Inorg. Met.-Org. Chem.* **1991**, *21*, 203.
11. (a) Birri, A.; Harvey, B.; Hogarth, G.; Subasi, E.; Ugur, F. *J. Organomet. Chem*. **2007**, *692*, 2448. (b) Gupta, R. K.; Pandey, R.; Singh, R.; Srivastava, N.; Maiti, B.; Saha, S.; Li, P.; Xu, Q.; Pandey, D. S. *Inorg. Chem*. **2012**, *51*, 8916. (c) Blake, A. J.; Kathirgamanathan, P.; Toohey, M. J. *Inorg. Chim. Acta* **2000**, *303*, 137.
12. (a) Feth, M. P. Klein, A.; Bertagnolli, H. *Eur. J. Inorg. Chem.* **2003**, 839. (b) Halimehjani, A. Z.; Marjani, K.; Ashouri, A.; Amani, V. *Inorg. Chim. Acta* **2011**, *373*, 282.
13. Sreedaran, S.; Bharathi, K. S.; Rahiman, A. K.; Jagadish, L.; Kaviyarasan, V.; Narayanan, V. *Polyhedron* **2008**, *27*, 2931.
14. Verma, S. K.; Singh, V. K. *Polyhedron* **2014**, *76*, 1.
15. (a) Lee, K.-H.; Choi, C.-S.; Jeon, K.-S. *J. Photosci.* **2002**, *9*, 71. (b) Martens, S. C.; Zschieschang, U.; Wadepohl, H.; Klauk, H.; Gade, L. H. *Chem. Eur. J.* **2012**, *18*, 3498. (c) Valdés, A. C.; P.-Luis, G.; Rivero, I. A. *J. Mex. Chem. Soc*. **2007**, *51*, 87. (d) Madrigal, D.; C.; P.-Luis, G.; Rivero, I. A. *J. Mex. Chem. Soc*. **2006**, *50*, 175. (e) Liu, H.; Li, B.; Liu, D.; Xu, Z. *Chem. Phys. Lett*. **2001**, *350*, 441. (f) Mizobe, Y.; Hinoue, T.; Yamamoto, A.; Hisaki, I.; Miyata, M.; Hasegawa, Y.; Tohnai, N. *Chem. Eur. J*. **2009**, *15*, 8175. (g) Reddy, D. R.; Maiya, B. G. *J. Porphyrins Phthalocyanines* **2002**, *06*, 3.
16. Davis, E. A.; Mott, N. F. *Phil. Mag*. **1970**, *22*, 903.
17. (a) Habibi, M. H.; Talebian, N. *Acta Chim. Slov*. **2005**, *52*, 53. (b) J. Tauc, *Mater. Res. Bull.* **1970**, *5*, 721.
18. (a) Sharma, R.; Kaushik, N. K. *J. Therm. Anal Calorim.* **2004**, *78*, 953. (b) Ali, B. F.; A.-Akramawi, W. S.; A.-Obaidi, K. H.; A.-Karboli, A. H. *Thermochim. Acta* **2004**, *419*, 39.
19. Memon, A. A.; Afzaal, M.; Malik, M. A.; Nguyen, C. Q.; O'Brien, P.; Raftery, J. *Dalton Trans.* **2006**, 4499.

20. Kumar, S. S.; Selvi, T. R. *Synth. React. Inorg. Met.-Org. Nano-Met. Chem.* **2008**, *38*, 710.
21. Onwudiwe, D. C.; Ajibade, P. A. *Int. J. Mol. Sci*. **2011**, *12*,1964.
22. (a) Kryatov, S. V.; Mohanraj, B. S.; Tarasov, V. V.; Kryatova, O. P.; R.-Akimova, E. V. *Inorg. Chem*. **2002**, *41*, 923. (b) Lai, C. S.; Tiekink, R. T. *Appl. Organomet. Chem.*, **2003**, *17*, 251. (c) Lai, C. S.; Tiekink, R. T. *Appl. Organomet. Chem.*, **2003**, *17*, 253.
23. (a) Ghosh, D.; Sen, K.; Das, A. K. *Struct Chem* **2012**, *23*, 227. (b) Yu, X.; Wang, N.; He, H.; Wang, L. *Spectrochim Acta A* **2014**, *122*, 283.
24. Frisch, M. J.; Trucks, G. W.; Schlegel, H. B.; Scuseria, G. E.; Robb, M. A.; Cheeseman, J. R.; Montgomery Jr., J. A.; Vreven, T.; Kudin, K. N.; Burant, J. C.; Millam, J. M.; Iyengar, S. S.; Tomasi, J.; Barone, V.; Mennucci, B.; Cossi, M.; Scalmani, G.; Rega, N.; Petersson, G. A.; Nakatsuji, H.; Hada, M.; Ehara, M.; Toyota, K.; Fukuda, R.; Hasegawa, J.; Ishida, M.; Nakajima, T.; Honda, Y.; Kitao, O.; Nakai, H.; Klene, M.; Li, X.; Knox, J. E.; Hratchian, H. P.; Cross, J. B.; Adamo, C.; Jaramillo, J.; Gomperts, R.; Stratmann, R. E.; Yazyev, O.; Austin, A. J.; Cammi, R.; Pomelli, C.; Ochterski, J. W.; Ayala, P. Y.; Morokuma, K.; Voth, G. A.; Salvador, P.; Dannenberg, J. J.; Zakrzewski, V. G.; Dapprich, S.; Daniels, A. D.; Strain, M. C.; Farkas, O.; Malick, D. K.; Rabuck, A. D.; Raghavachari, K.; Foresman, J. B.; Ortiz, J. V.; Cui, Q.; Baboul, A. G.; Clifford, S.; Cioslowski, J.; Stefanov, B. B.; Liu, G.; Liashenko, A.; Piskorz, P.; Komaromi, I.; Martin, R. L.; Fox, D. J.; Keith, T.; A.-Laham, M. A.; Peng, C. Y.; Nanayakkara, A.; Challacombe, M.; Gill, P. M. W.; Johnson, B.; Chen, W.; Wong, M. W.; Gonzalez, C.; Pople, J. A.; Gaussian, Inc., Wallingford, CT, **2004**.
25. (a) Beer, P. D.; Berry, N. G.; Cowley, A. R.; Hayes, E. J.; Oates, E. C.; Wong, W. W. H. *Chem. Commun*., **2003**, 2408. (b) Wong, W. W. H.; Curiel, D.; Lai, S.-W.; Drew, M. G. B.; Beer, P. D. *Dalton Trans*., **2005**, 774.
26. (a) Gadre, S. R.; Bhadane, P. K. *Resonance*, **1999**, *4*, 11. (b) Bulat, F. A.; T.-Labbé, A.; Brinck, T.; Murray, J. S.; Politzer, P. *J Mol Model* **2010**, *16*, 1679. (c) Politzer, P.; Laurence, P. R.; Jayasuriya, K. *Environ. Health Perspect.* **1985**, *61*, 191.

27. Vladimirova, K. G.; Freidzon, A. Y.; Kotova, O. V.; Vaschenko, A. A.; Lepnev, L. S.; Bagatur'yants, A. A.; Vitukhnovskiy, A. G.; Stepanov, N. F.; Alfimov M. V. *Inorg. Chem.*, **2009**, *48*, 11123.
28. (a) Driggers, E.M.; Hale, S. P.; Lee, J.; Terrett, N. K. *Nat. Rev. Drug Discov.* **2008**, *7*, 608. (b) Mallinson, J.; Collins, I. *Future Med. Chem.* **2012**, *4*, 1409. (c) Mann A. Conformational restriction and/or steric hindrance in medicinal chemistry. In: *The Practice Of Medicinal Chemistry*, Wermuth CG (Ed.). Academic Press, London, UK 2008.
29. Ferreira, I. P.; de Lima, G. M.; Paniago, E. B.; Rocha, W. R.; Takahashi, J. A.; Pinheiro, C. B.; Ardisson, J. D. *Eur. J. Med. Chem.* **2012**, *58*, 493.
30. Wang, L.; Wang, X.; Chen, X.; Liu, J.; Liu, S.; Zhao, C. Bioelectrochemistry **2012**, *88* 30.
31. (a) Orvig, C.; Abrams, M. J. *Chem. Re*v.**1999**, *99 (Special Issue)*, 2201. (b) Ronconi, L.; Marzano, C.; Zanello, P.; Corsini, M.; Miolo, G.; Maccá, C.; Trevisan, A.; Fregona, D. *J. Med. Chem.* **2006,** *49*, 1648.
32. (a) Bach, S. P.; Chinery, R.; O'Dwyer, S. T.; Potten, C. S.; Coffey, R. J.; Watson, A. J. *Gastroenterology* **2000**, *118*, 81. (b) Daniel, K. G.; Chen, D.; Orlu, S.; Cui, Q. C.; Miller, F. R.; Dou, Q. P. *Breast Cancer Res.* **2005**, *7*, R897. (c) Segovia, N.; Crovetto, G.; Lardelli, P.; Espigares, M. J. Appl. Toxicol. 2002, 22, 353. (d) Viquez, O. M.; Valentine, H. L.; Amarnath, K.; Milatovic, D.; Valentine, W. M. Toxicol. Appl. Pharmacol. 2008, 229, 77. (e) Chabicovsky, M.; P.-Grassauer, E.; Seipelt, J.; Muster, T.; Szolar, O. H. J.; Hebar, A.; Doblhoff-Dier, O. Basic Clin. Pharmacol. Toxicol. 2010, 107, 758. (f) Nagy, E. M.; Sitran, S.; Montopoli, M.; Favaro, M.; Marchiò, L.; Caparrotta, L.; Fregona, D. *J Inorg. Biochem*. **2012**, *117*, 131. (g) Qian, Y.; Ma, G.-Y.; Yang, Y.; Cheng, K.; Zheng, Q.-Z.; Mao, W.-J.; Shi, L.; Zhao, J.; Zhu, H.-L. *Bioorg. Med. Chem*. **2010**, *18*, 4310.
33. (a) Takeshima, T.; Ikeda, M.; Yokoyama, M.; Fukada, N.; Muraoka, M. *J. Chem. Soc., Perkin* **1979**, *1*, 692. (b) Beaty, J. A.; Jones, M. M.; Wilson, D. J.; Ma, L. *Chem. Res. Toxicol.* **1992**, *5*, 568.
34. (a) Amarnath, V.; Amarnath, K.; Valentine, W. M. *Curr. Top. Toxicol.* **2007**, *4*, 39. (b) Garcia, J. I.; Humeres, E. *J. Org. Chem.* **2002**, *67*, 2755. (c) Humeres, E.; Debacher, N. A.; Franco, J. D.; Lee, B. S.; Martendal, A. *J. Org. Chem.* **2002**, *67*,

3662. (d) Humeres, E., Debacher, N. A., and Sierra, M. M. *J. Org. Chem.* **1999**, *64*, 1807.

5B.6. Annexure

Spectral Characterization

Mass Spectra:

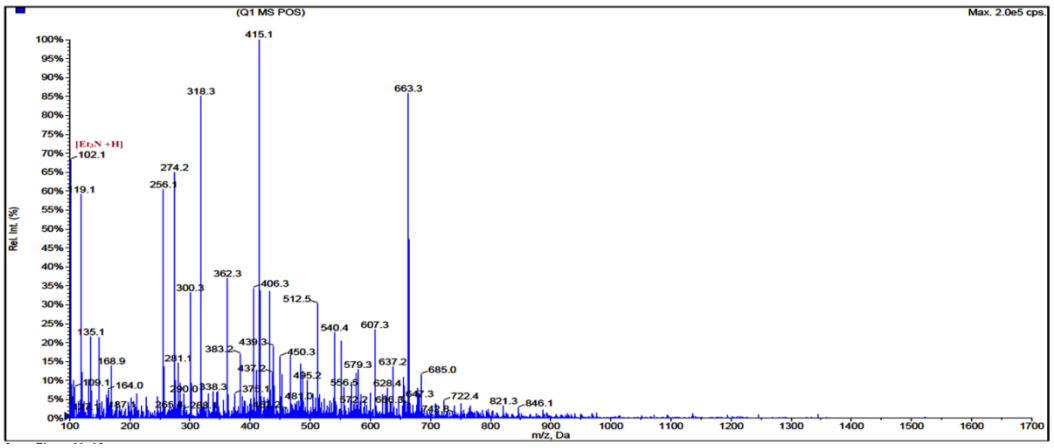

Annexure 1. Mass spectrum (positive ion mode) of complex **1**.

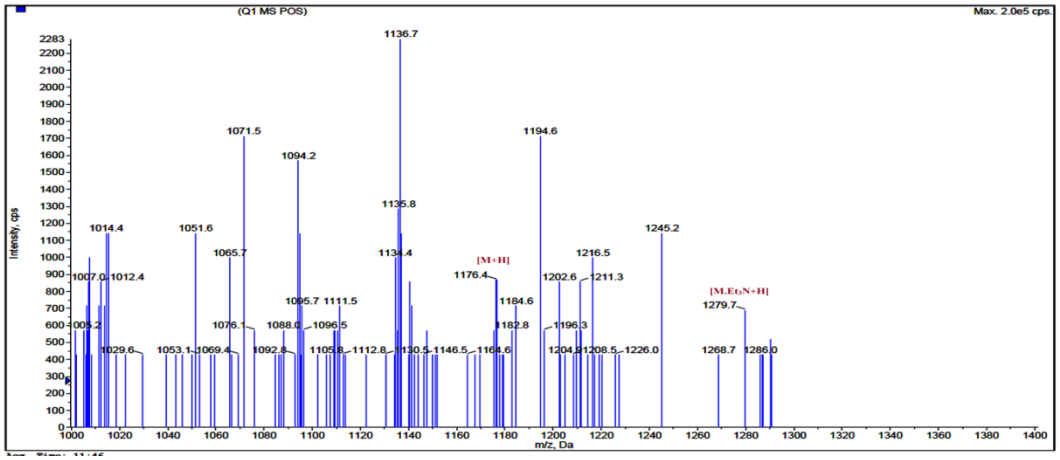

Annexure 2. Mass spectrum (positive ion mode) of complex **1.**

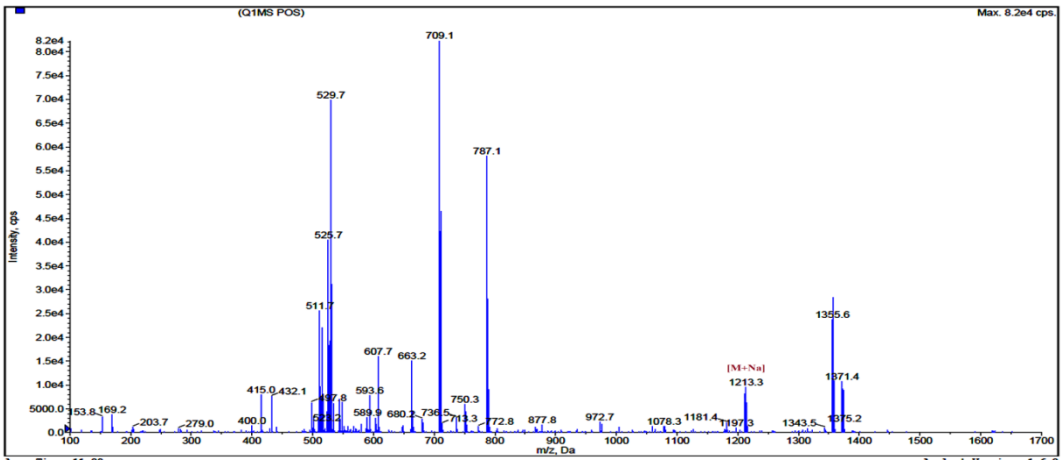

Annexure 3. Mass spectrum (positive ion mode) of complex **2**.

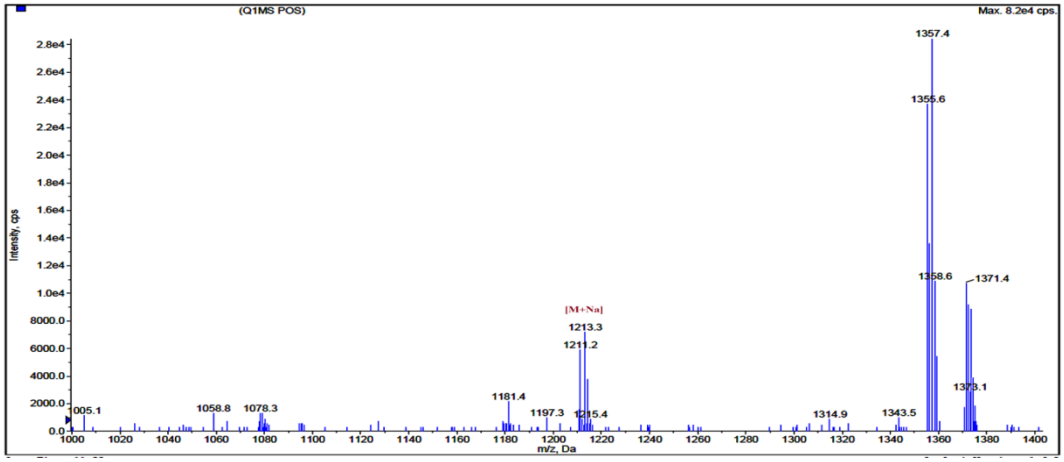

Annexure 4. Mass spectrum (positive ion mode) of complex **2**.

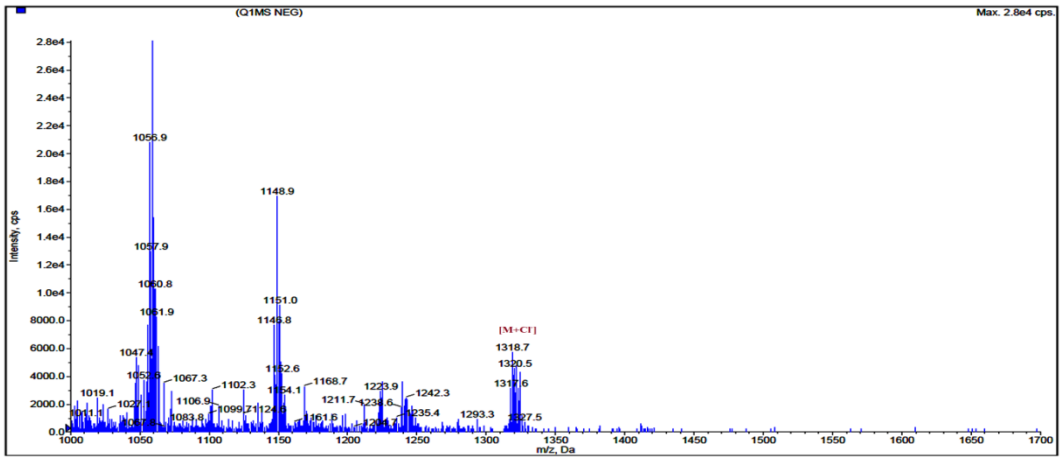

Annexure 5. Mass spectrum (negative ion mode) of complex **3**.

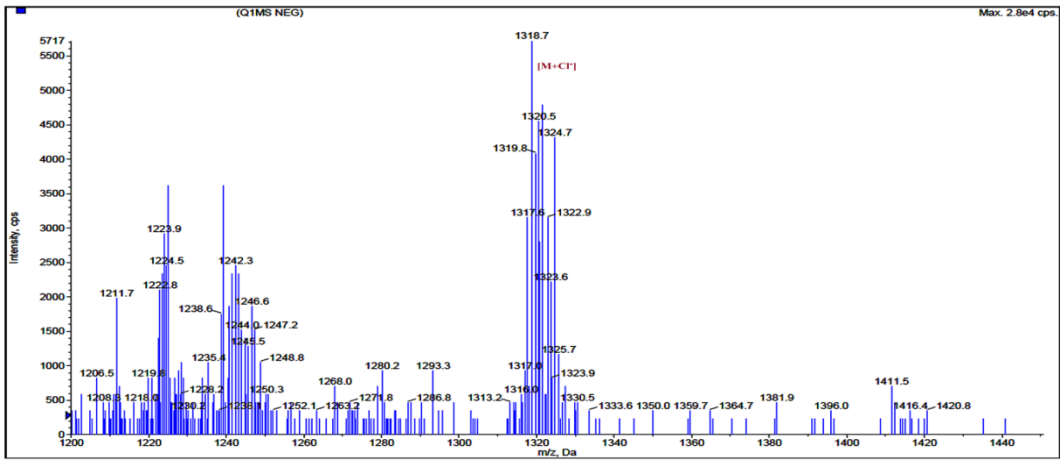

Annexure 6. Mass spectrum (negative ion mode) of complex **3**.

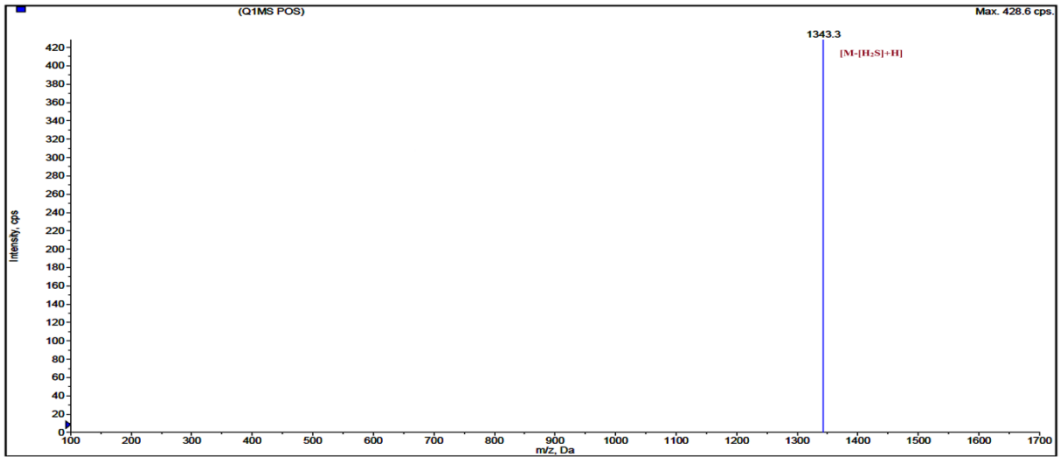

Annexure 7. Mass spectrum (positive ion mode) of complex **4**.

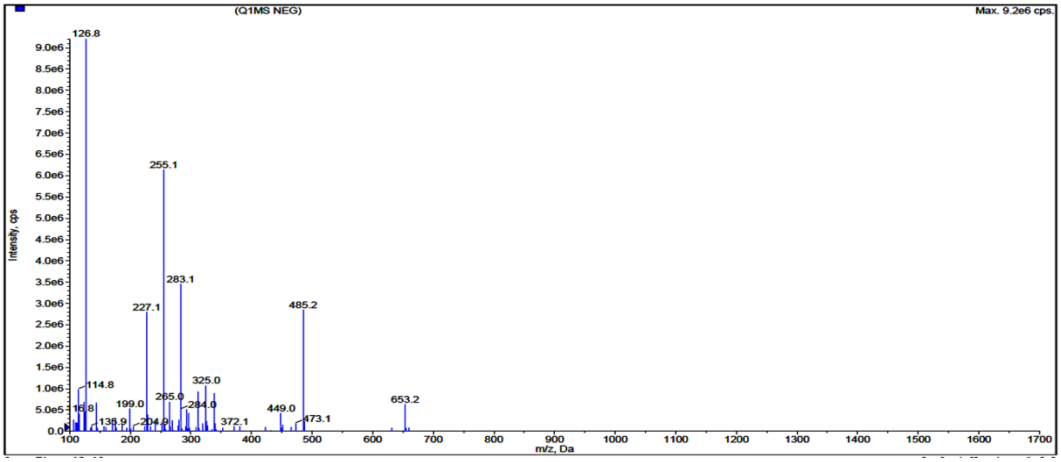

Annexure 8. Mass spectrum (negative ion mode) of complex **4**.

Table A1 Mass Analysis of binuclear M^{II}dithiocarbamate complexes (**1-4**)

m/z	**Possible fragments**
	Complex 1 (1175.99)
1279.7	[M.Et_3N+H]
1194.6	[M+19] (19: NH_4/H_3O)
1176.4	[M+H]

663.3

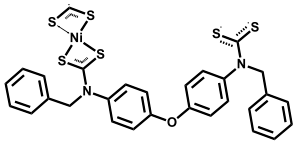

512.5

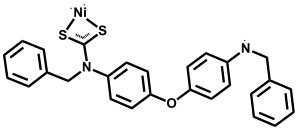

391.91

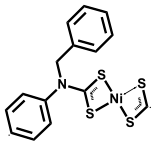

415.91 [391.91 + 23]

102.1 [Et_3N+H]

Complex 2 (1187.98)

1356.58 [M + diphenylether]

1213.3 [M+Na]

709.1 [699.05 +3Li+H]

699.05

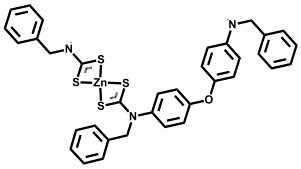

593.6 Symmetrical cleavage

102.1 No peak for Et_3N

Complex 3 (1287.93) (negative ion mode)

1320.5 1285.93 + Cl^-

1148.9 [1058+benz+H^-]

1022.14

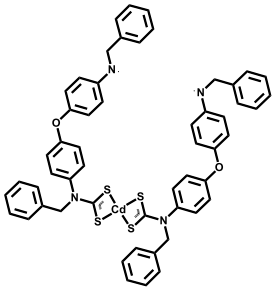

1058 [1022.14 + Cl^-]

OR

[M-(Cd+2CS_2)+Cl^-]

Complex 4 (1376.06)

1343.3 [(M-S) + H]

653.2 [630.09 + 23]

630.09

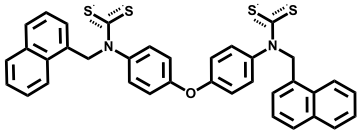

485.2 [478.20 + 2Li+ H^-]

478.20

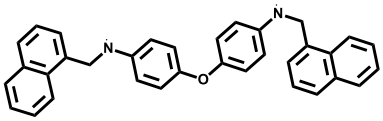

255.1 [254.02 + H^-]

254.02 [231.02 + 23]

231.02

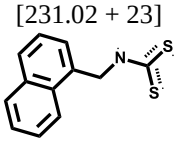

126.8

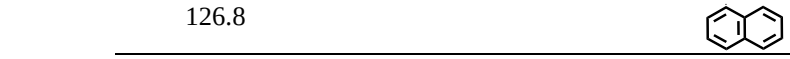

1. IR spectra

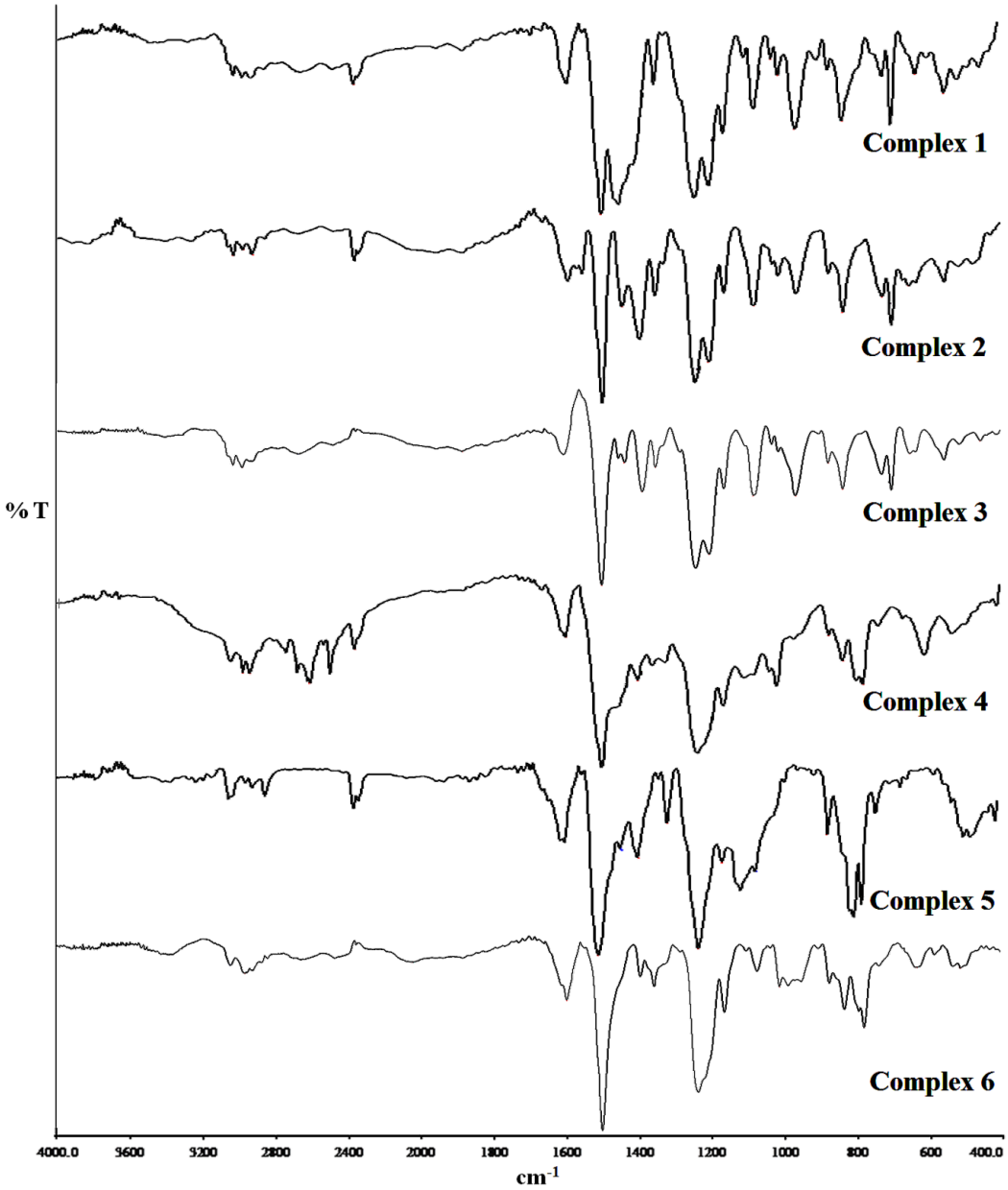

Annexure 9. IR spectra of complex **1-6**.

2. NMR spectra

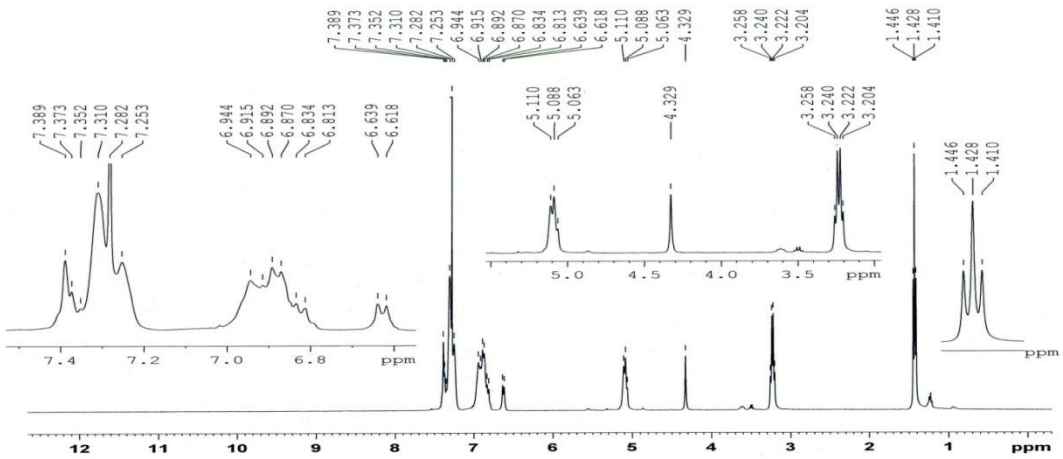

Annexure 10. ^{1}H NMR spectrum of complex **1**.

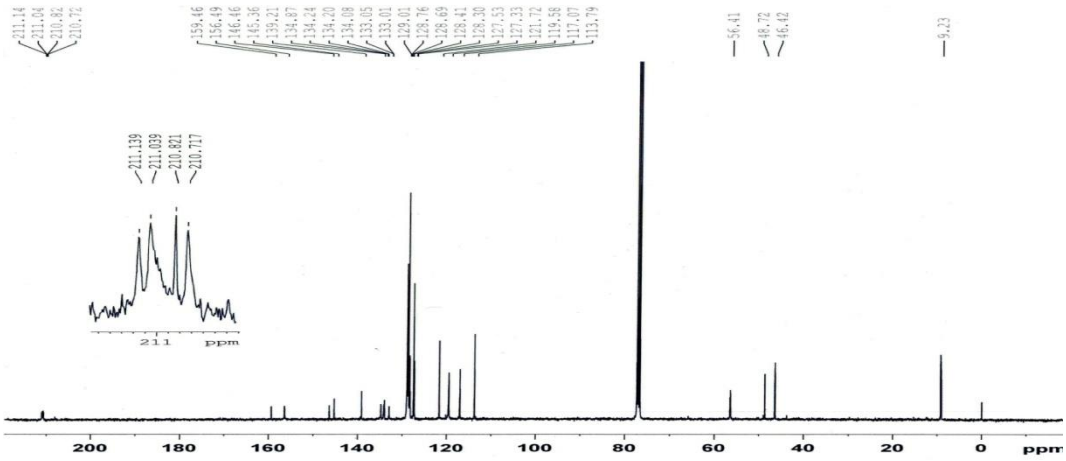

Annexure 11. ^{13}C NMR spectrum of complex **1**.

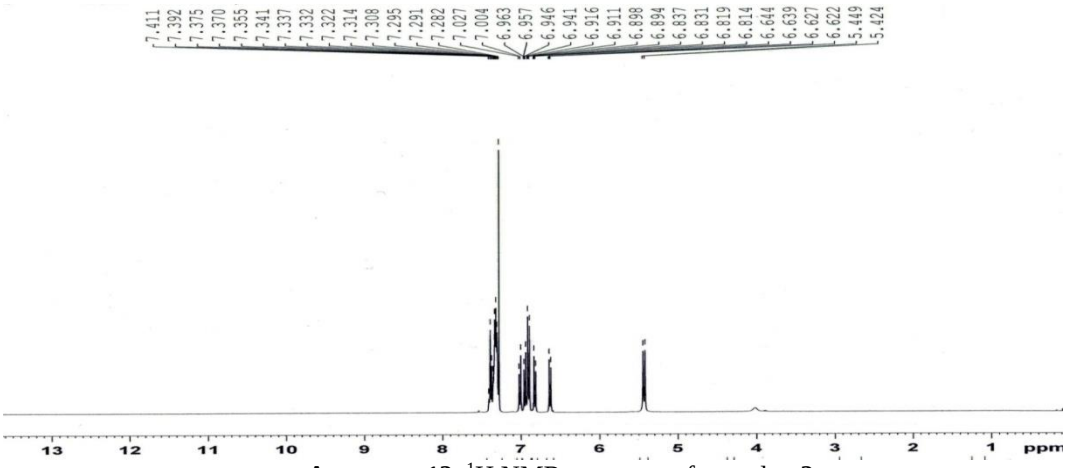

Annexure 12. ^{1}H NMR spectrum of complex **2**.

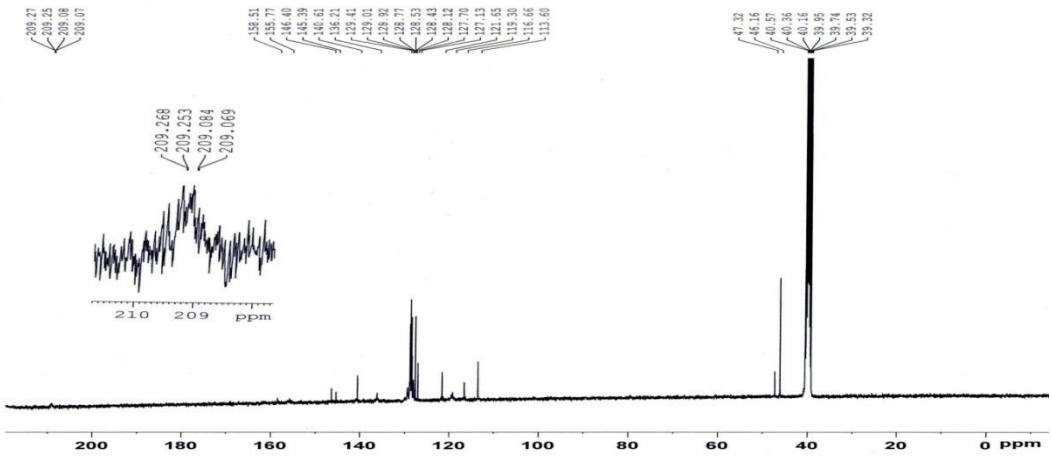

Annexure 13. ^{13}C NMR spectrum of complex **2**.

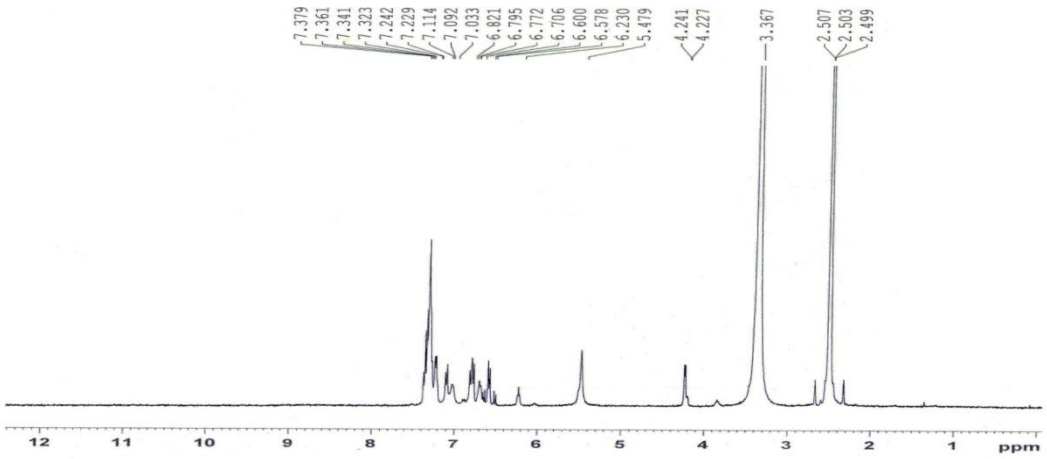

Annexure 14. ^{1}H NMR spectrum of complex **3**.

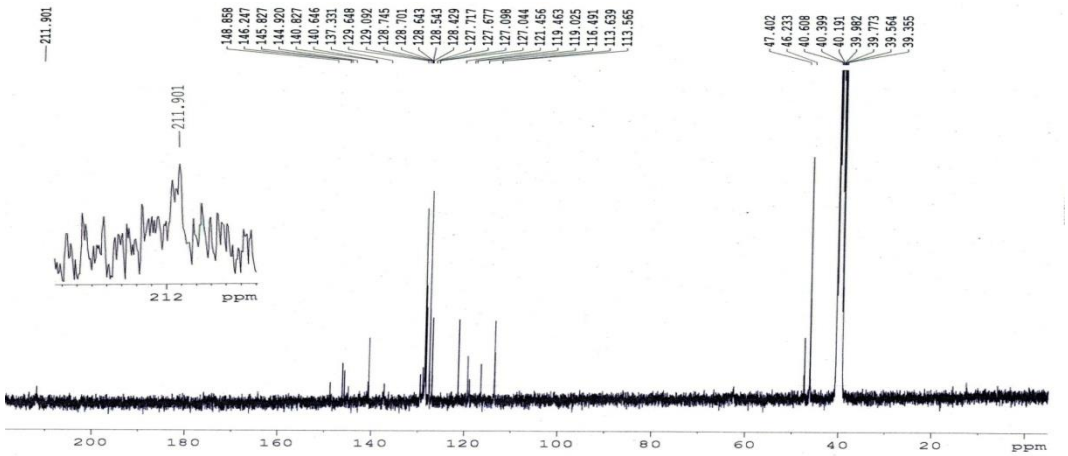

Annexure 15. ^{13}C NMR spectrum of complex **3**.

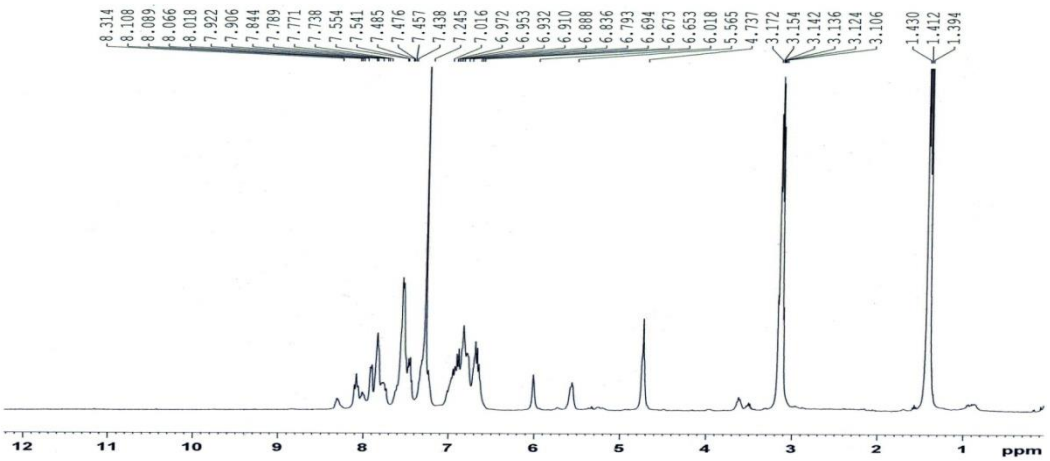

Annexure 16. ^{1}H NMR spectrum of complex **4**.

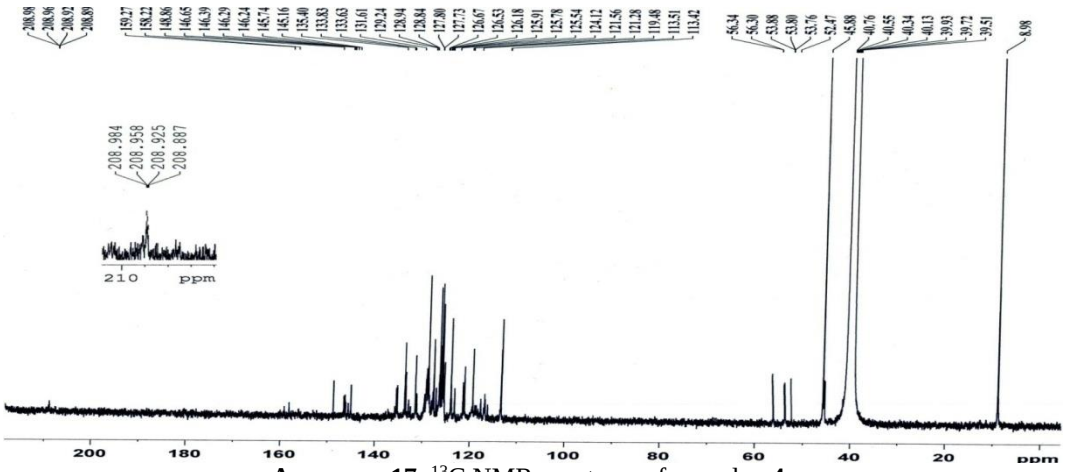

Annexure 17. ^{13}C NMR spectrum of complex **4**.

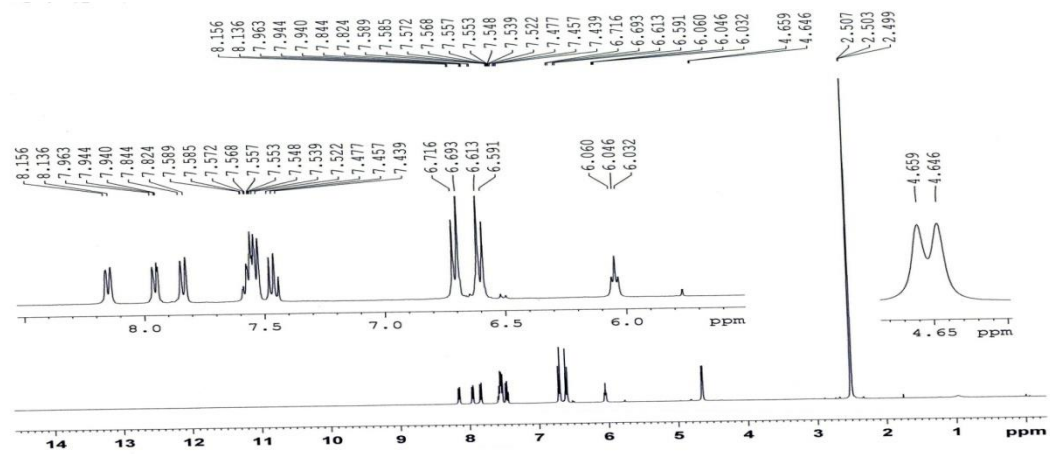

Annexure 18. ^{1}H NMR spectrum of complex **5**.

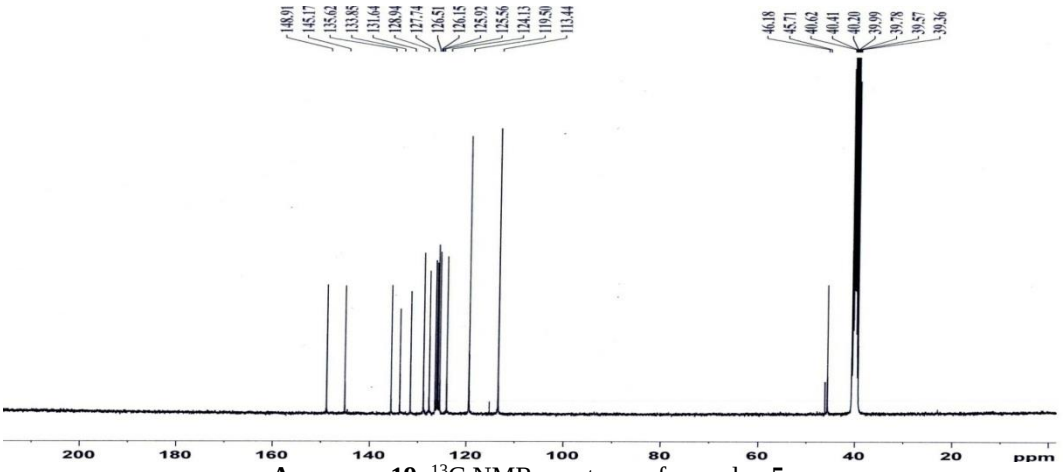

Annexure 19. ^{13}C NMR spectrum of complex **5**.

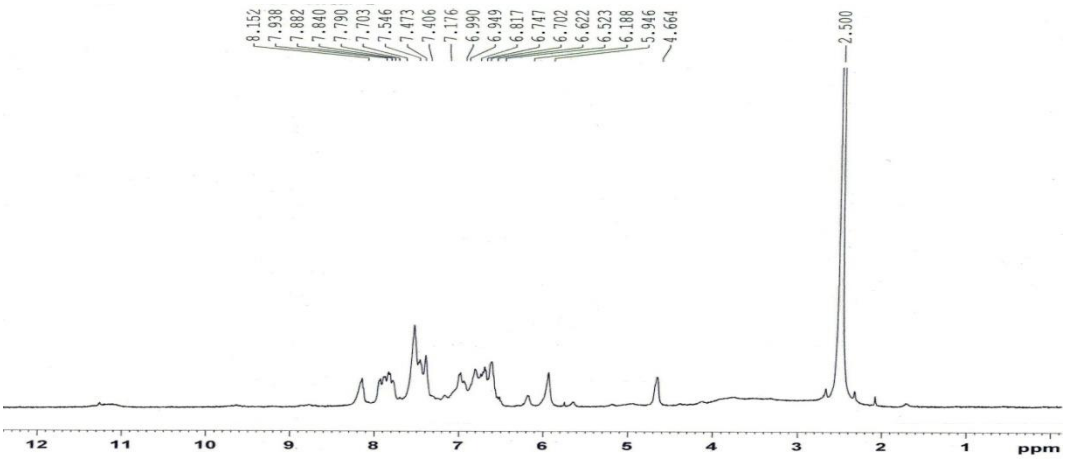

Annexure 20. ^{1}H NMR spectrum of complex **6**.

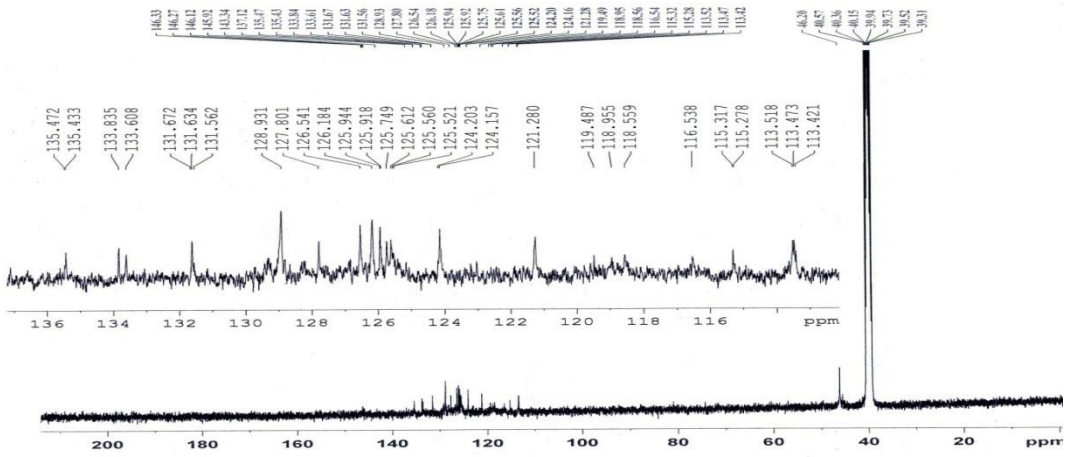

Annexure 21. ^{13}C NMR spectrum of complex **6**.

Optical Properties

i. UV-Visible Absorption

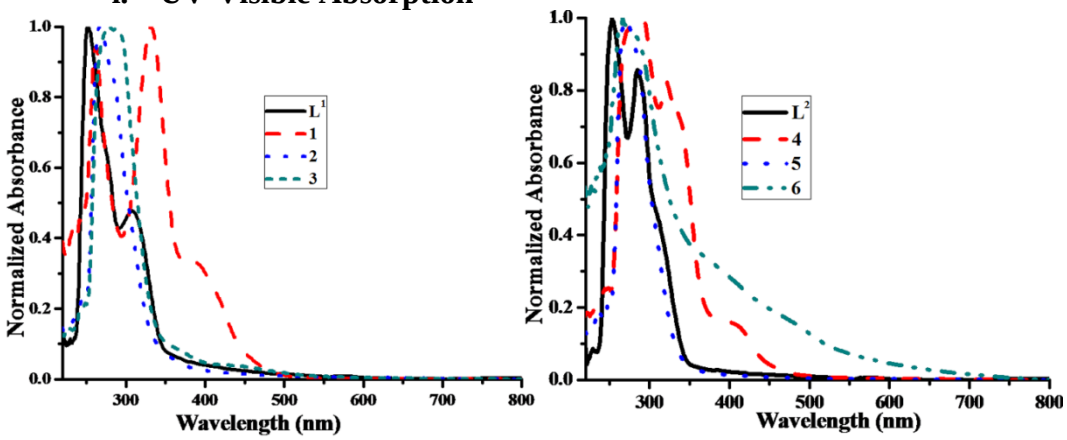

Annexure 22. UV–visible absorption spectra of compounds **L[1]**, **L[2]** and **1-6** in 10^{-5} M DMSO solution.

ii. UV-Visible Emission

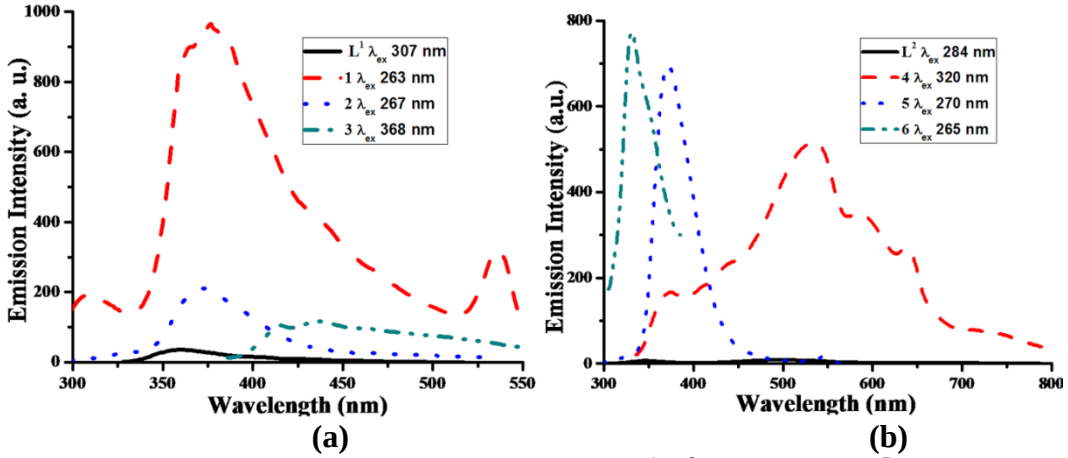

Annexure 23. UV–visible emission spectra of compounds **L[1]**, **L[2]** and **1-6** from 10^{-5} M DMSO solution.

iii. Uv-visible transmittance (Optical Band gap)

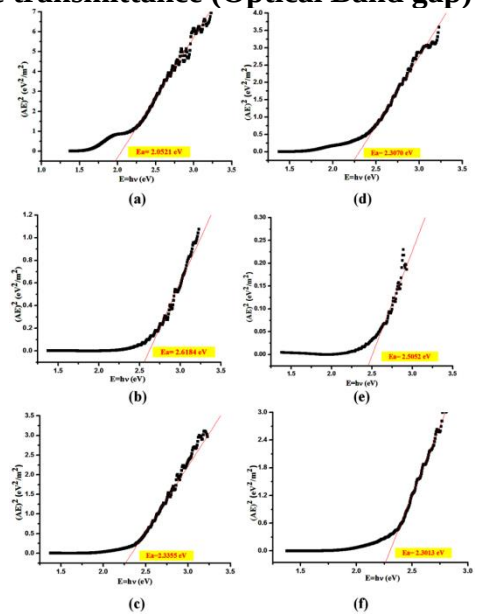

Annexure 24. Tauc plot illustrating the optical band gap for **1-6** by UV–visible transmittance study.

Thermogravimetric Study

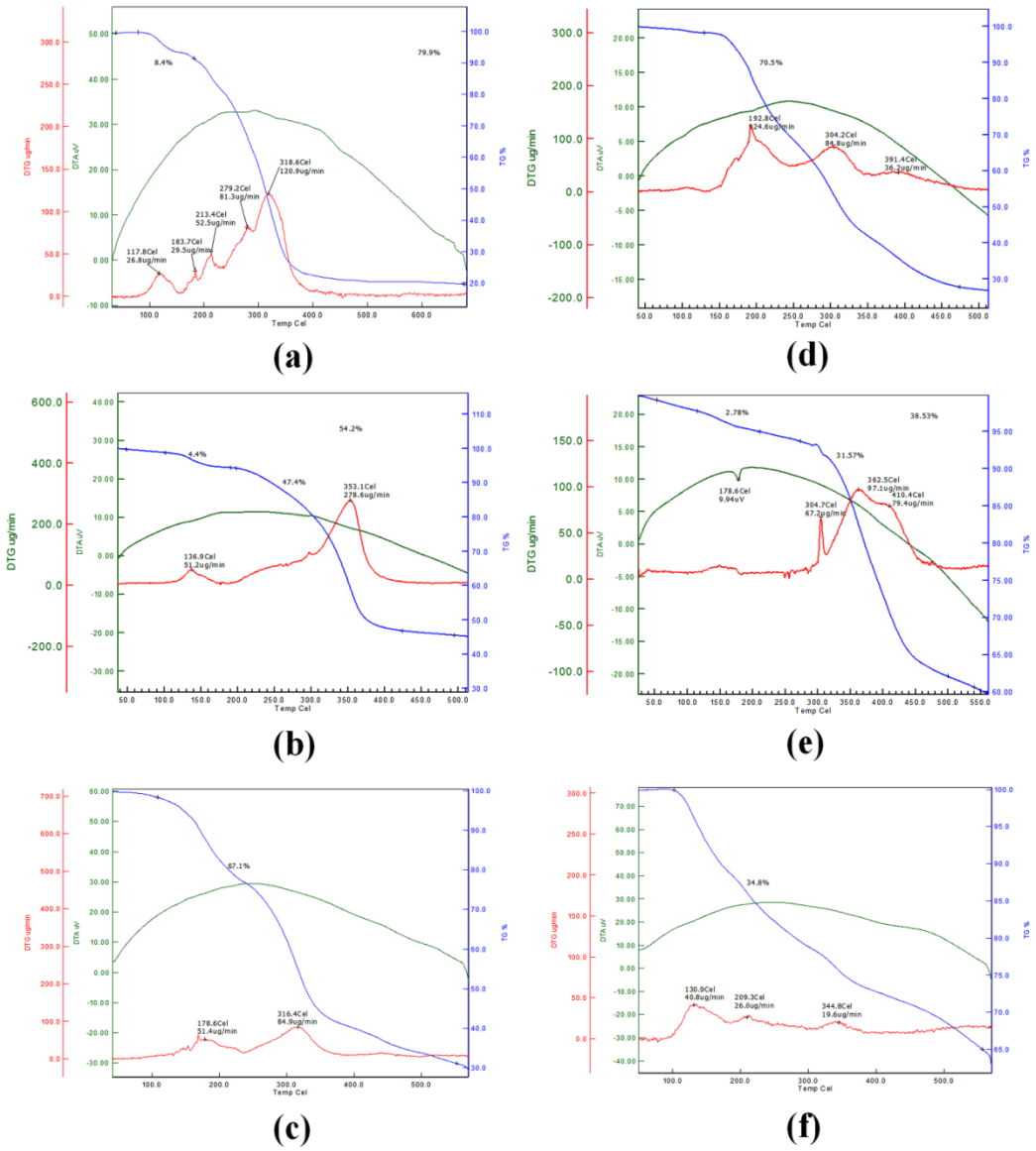

Annexure 25.TGA/DTA plots, (a-f): for binuclear complex **1-6**.

Table A2. Thermogravimetric data for **1-6**.

Compounds	Mass Loss% (Temperature °C)	DTG (°C)	Residual content (%)	Inference
1	8.4% (100-150) 79.9% (100-700)	117.8 (26.8), 183.7 (29.5), 213.4 (52.5), 279.2 (81.3), 318.6 (120.9)	20.1	1st stage: loss of Et_3N molecules (calc. 7.8 %). 2nd -4th stage: continuous mass loss of ligand framework. - at 400 °C stable residual mass obtained which corresponds to NiS (14.18 %) and char (5.92 %). - Maximum rate of decomposition observed at 318.6 °C on DTG curve.
2	4.4% (100-200) 47.4% (200-450) 54.2% (100-500)	136.9 (51.2), 353.1 (278.6)	45.8	1st stage: insignificant mass loss of solvent impurities. 2nd stage: continues mass loss of ligand framework even at 550 °C. - Maximum rate of decomposition observed at 353.1 °C on DTG curve.
3	67.1% (120-550)	178.6 (51.4), 316.4 (84.9)	32.9	1st -2nd stage: continues mass loss of ligand framework even at 550 °C. - Maximum rate of decomposition observed at 316.4 °C on DTG curve.
4	70.5% (120-500)	192.8(124.6), 304.2(84.8), 319.4(36.2)	29.5	Thermally stable up to 150 °C. 1st -3rd stage: Continuous thermal decomposition which continues after 550 °C. - at 550 °C residual mass obtained which corresponds to NiS (12.26 %) and char (17.24 %). - Maximum rate of decomposition observed at 192.8 °C on DTG curve.
5	2.78% (100-200) 31.57% (280-500) 38.53% (100-500)	304.7(312.3), 362.5(97.1), 410.4(79.4)	61.47	1st -3rd stage: continues mass loss of ligand framework even at 550 °C. - Maximum rate of decomposition observed at 304.7 °C on DTG curve.
6	34.8% (120-550)	130.9(40.8), 209.3(26.0), 344.8(19.6)	65.2	1st -3rd stage: continues mass loss of ligand framework even at 550 °C. - Maximum rate of decomposition observed at 130.9 °C on DTG curve.

Host-Guest Interactions

The host-guest binding ability of some of the macrocyclic complexes (**1-4**) was explored towards a number of guest species viz. 1,4-dioxane, 4,4'-bipyridine, piperazine and triethyl amine by Job plot experiments using UV-vis absorption spectrophotometry.

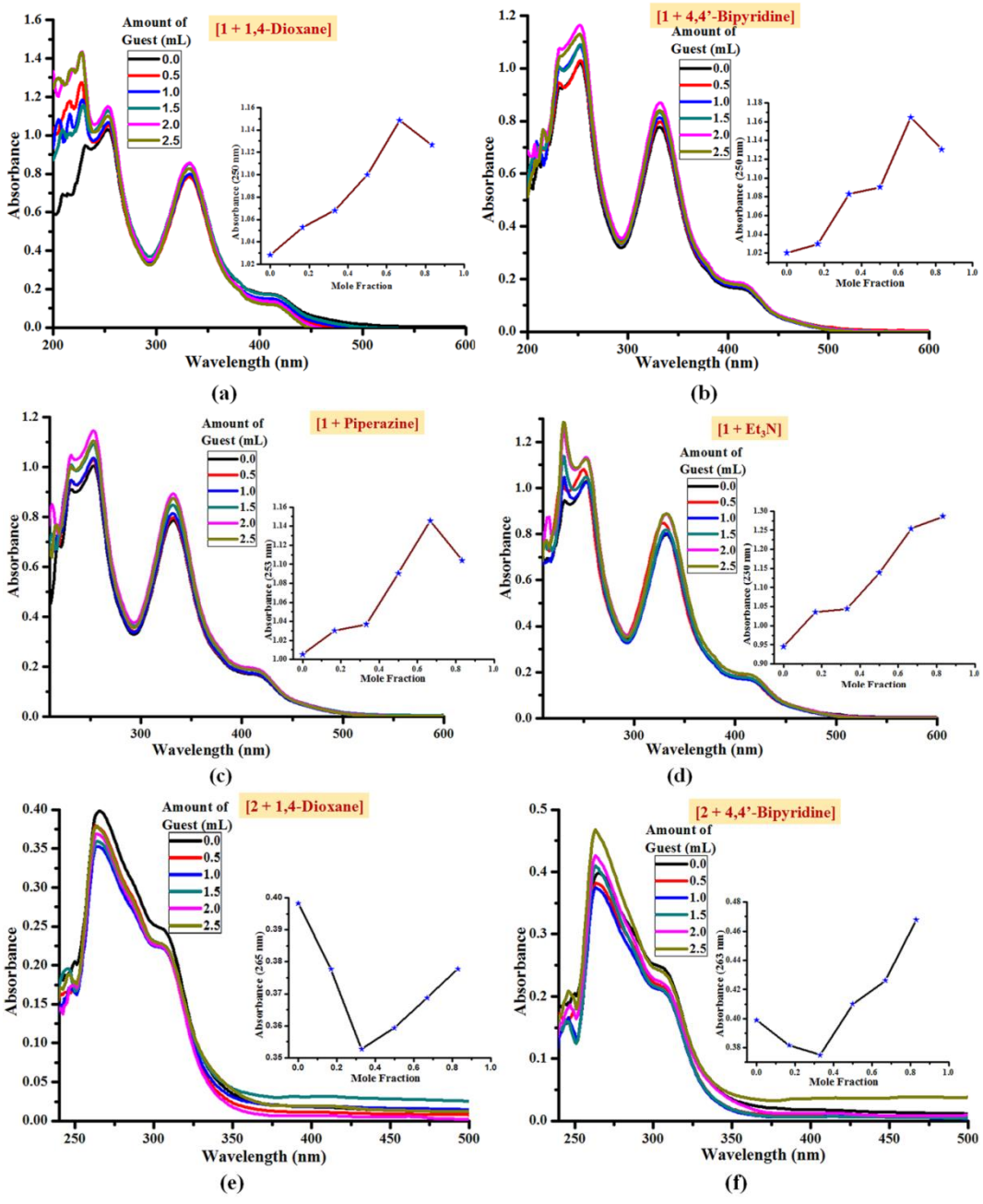

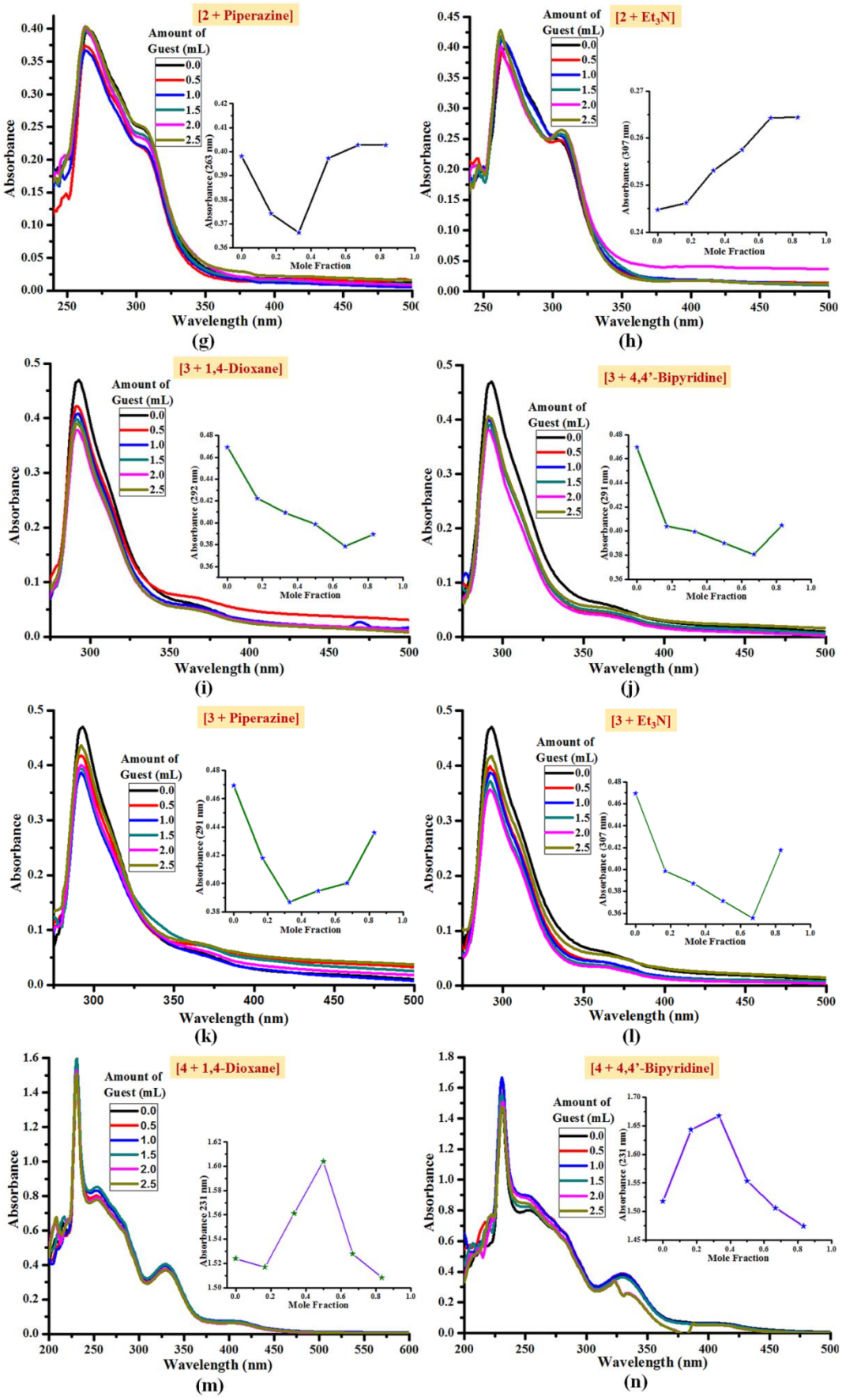
[2 + Piperazine]
Amount of Guest (mL)
0.0
0.5
1.0
1.5
2.0
2.5
Absorbance
Wavelength (nm)
Absorbance (263 nm)
Mole Fraction
(g)
[2 + Et3N]
Absorbance (307 nm)
(h)
[3 + 1,4-Dioxane]
Absorbance (292 nm)
(i)
[3 + 4,4'-Bipyridine]
Absorbance (291 nm)
(j)
[3 + Piperazine]
(k)
[3 + Et3N]
Absorbance (307 nm)
(l)
[4 + 1,4-Dioxane]
Absorbance 231 nm)
(m)
[4 + 4,4'-Bipyridine]
Absorbance (231 nm)
(n)

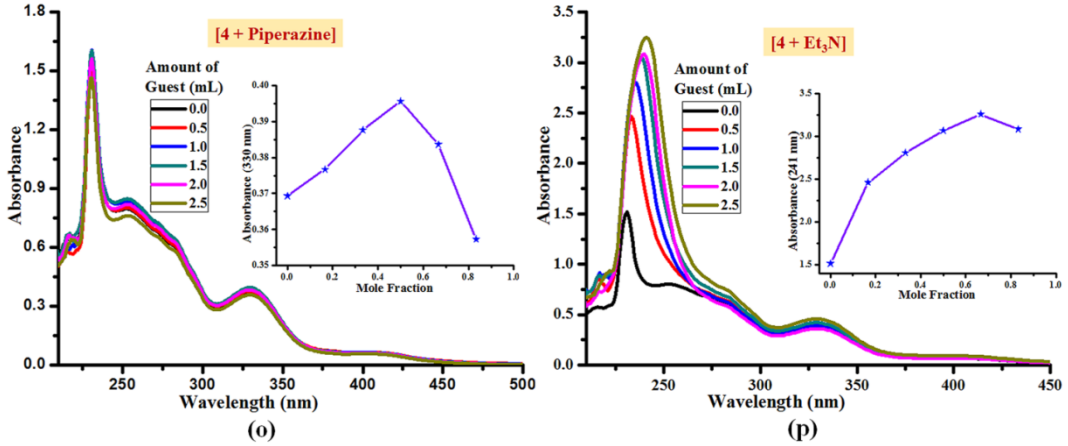

Annexure 26. UV-visible absorption spectral change in Job Plot experiments of **1-4** with various guests. Inset shows the Job Plot for the interaction between hosts and guests consistent with 1:1 (m, o); 1:2 (a-c, i, j. l, p) and 2:1 (e-g, k, n) (host : guest) binding stoichiometries.

Computational Investigation

i. Molecular Electrostatic Potential (MESP)

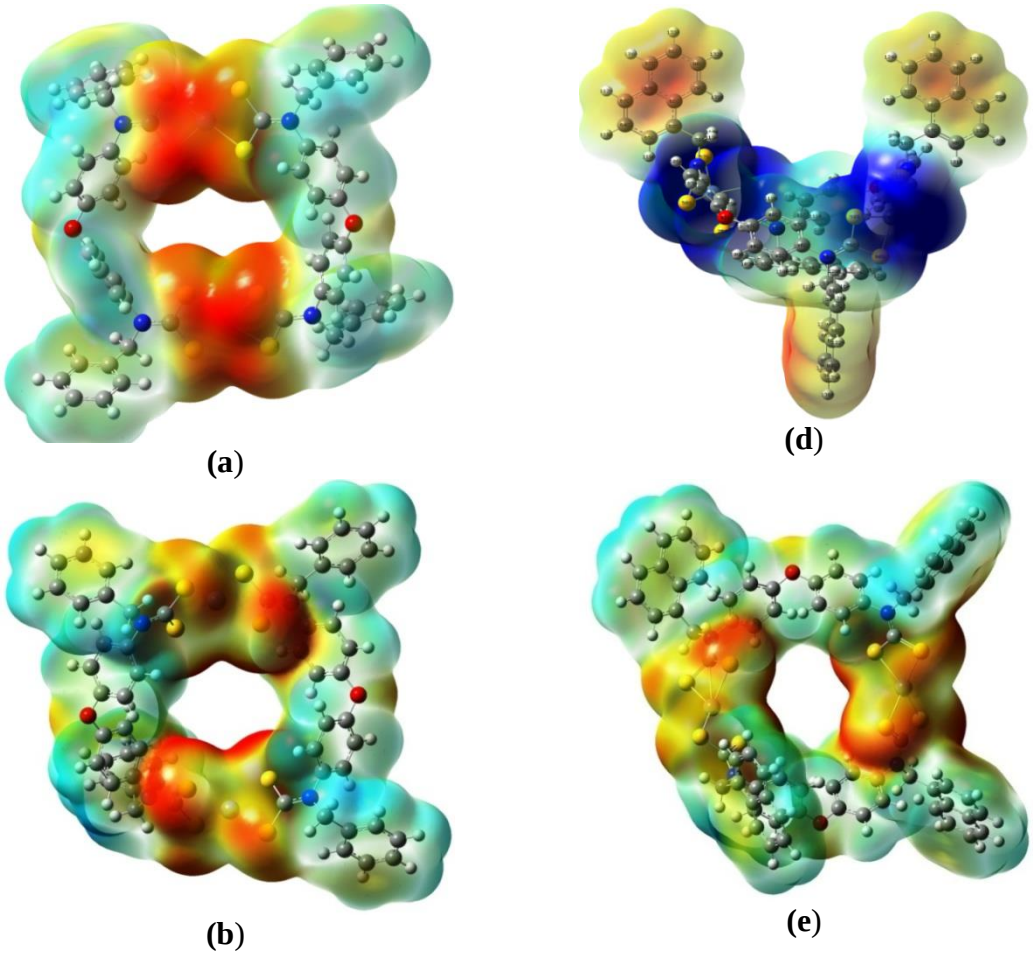

(a) **(d)**

(b) **(e)**

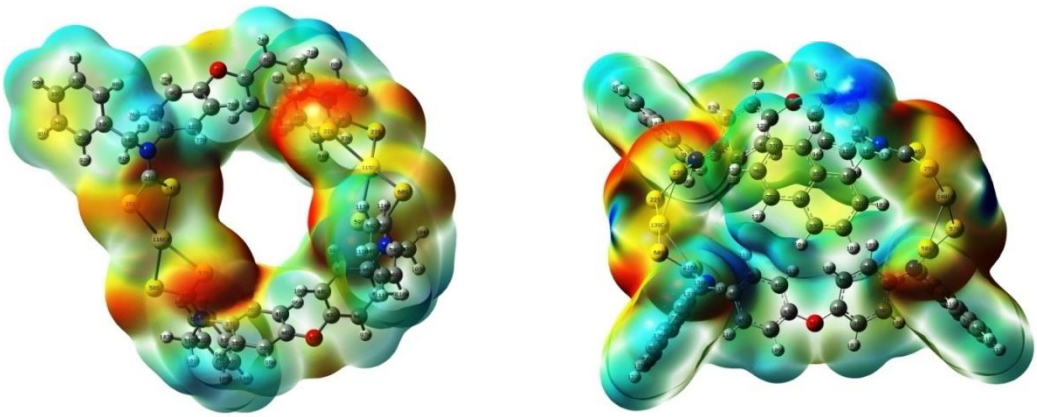

(c) **(f)**

Annexure 27. Graphical representation of electron density from total SCF density (isoval= 0.0004; mapped with ESP, Red and blue colour represents localization of negative and positive potential respectively) for compounds **1** (a); **2** (b); **3** (c); **4** (d); **5** (e) and **6** (f).

2.6.5. Cytotoxic Activity

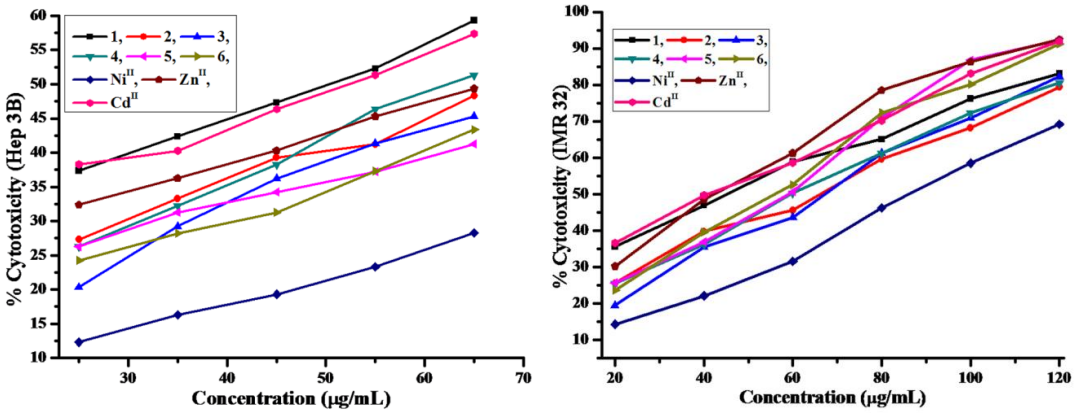

(a) **(b)**

Annexure 28. Cytotoxicity (%) of **1-6** and $M(OAc)_2$ against (a) **HEP 3B** (b) **IMR 32** cell lines.

Table A11. Parameters obtained from the computational investigations and cytotoxic activity for electronic models.

Entry	E_{HOMO} (eV)	E_{LUMO} (eV)	ΔE_{H-L} (eV)	Charges on 'N' and chelated 'N-CSS-M' atoms	M...M distance (Å)	Dipole moment (Debye)
L^1	-4.7782	-0.1967	4.5814	N: - (0.606-0.607)	...	1.4188
L^2	-4.8478	-1.1048	3.7430	N: - (0.626)	...	1.1360
1	-5.4797	-1.8023	3.6774	Ni: - (0.251) S: - (0.024-0.025) C: - (0.021-0.024) N: - (0.380-0.383)	9.959	1.7025
2	-5.8823	-1.0795	4.8028	Zn: (0.540-0.541) S: - (0.179-0.215) C: - (0.029-0.031) N: - (0.371-0.372)	10.402	1.0026
3	*-5.7836*	-1.0719	4.7118	Cd: (0.593) *S: - (0.191-0.226)* C: - (0.024-0.026) N: - (0.374-0.375)	10.494	0.8335
4	- 5.7251	- 2.2602	3.4649	Ni: - (0.259-0.270) S: - (0.007-0.029) C: - (0.040-0.056) N: - (0.365-0.391)	12.205	2.1458
5	- 5.8285	- 1.2909	4.5376	Zn: (0.536-0.542) *S: - (0.182-0.216)* C: - (0.027-0.041) N: - (0.368-0.391)	10.476	0.9716
6	- 5.5921	- 1.8183	3.7738	Cd: (0.566-0.570) S: - (0.179-0.206) C: - (0.043-0.059) N: - (0.369-0.396)	13.682	2.1231